Meteoritics & Planetary Science 35, 1365–1386 (2000)

Evidence for low-temperature growth of fayalite and hedenbergite in MacAlpine Hills 88107, an ungrouped carbonaceous chondrite related to the CM-CO clan

ALEXANDER N. KROT[1]*, ADRIAN J. BREARLEY[2], MICHAEL I. PETAEV[3], GREGORY W. KALLEMEYN[4], DEREK W. G. SEARS[5], PAUL H. BENOIT[5], IAN D. HUTCHEON[6], MICHAEL E. ZOLENSKY[7] AND KLAUS KEIL[1]

[1]Hawaii Institute of Geophysics and Planetology, School of Ocean and Earth Science and Technology, University of Hawaii, Honolulu, Hawaii 96822, USA
[2]Earth and Planetary Sciences, University of New Mexico, Albuquerque, New Mexico 87131, USA
[3]Harvard-Smithsonian Center for Astrophysics, Cambridge, Massachusetts 02138, USA
[4]Tokyo Metropolitan University, Department of Chemistry, Graduate School of Science, Tokyo 192-0397, Japan
[5]Department of Chemistry and Biochemistry, University of Arkansas, Fayetteville, Arkansas 72701, USA
[6]Lawrence Livermore National Laboratory, Livermore, California 94551, USA
[7]Mail Code SN2, NASA Johnson Space Center, Houston, Texas 77058, USA
*Correspondence author's e-mail address: sasha@pgd.hawaii.edu

(Received 2000 February 16; accepted in revised form 2000 August 21)

Abstract–The carbonaceous chondrite MacAlpine Hills (MAC) 88107 has bulk composition and mineralogy that are intermediate between those of CO and CM chondrites. This meteorite experienced minor alteration and a low degree of thermal metamorphism (petrologic type 3.1) and escaped post-accretional brecciation. The alteration resulted in the formation of fayalite ($Fa_{90–100}$), Al-free hedenbergite ($\sim Fs_{50}Wo_{50}$), phyllosilicates (saponite-serpentine intergrowths), magnetite, and Ni-bearing sulfides (pyrrhotite and pentlandite). Fayalite and hedenbergite typically occur as veins, which start at the opaque nodules in the chondrule peripheries, crosscut fine-grained rims and either terminate at the boundaries with the neighboring fine-grained rims or continue as layers between these rims. These observations suggest that fayalite and hedenbergite crystallized after accretion and compaction of the fine-grained rims. Fayalite also overgrows isolated forsteritic ($Fa_{1–5}$) and fayalitic ($Fa_{20–40}$) olivine grains without any evidence for Fe-Mg interdiffusion; it also replaces massive magnetite-sulfide grains. The initial $^{53}Mn/^{55}Mn$ ratio of $(1.58 \pm 0.26) \times 10^{-6}$ in the MAC 88107 fayalite corresponds to an age difference between the formation of fayalite and refractory inclusions in Allende of either ~9 or 18 Ma, depending upon the value of the solar system initial abundance of ^{53}Mn used in age calculations.

Formation of secondary fayalite and hedenbergite requires mobilization and transport of Ca, Si, and Fe either through a high-temperature gaseous phase (Hua and Buseck, 1995) or low-temperature aqueous solution (Krot *et al.*, 1998a,b). The high-temperature nebular model for the origin of fayalite (Hua and Buseck, 1995) fails to explain (a) formation of fayalite–hedenbergite assemblages after accretion of fine-grained rims that lack any evidence for high-temperature processing; (b) extreme fractionation of refractory lithophile elements of similar volatility, Ca and Al, in hedenbergite; and (c) absence of Fe-Mg interdiffusion along fayalite–forsterite boundaries. We conclude that fayalite and hedenbergite in MAC 88107 formed during late-stage, low-temperature (approximately 150–200 °C) aqueous alteration. The data for MAC 88107 extend the evidence for an early onset of aqueous activity on chondrite parent bodies and reinforce the conclusion that liquid water played an important role in the chemical and mineralogical evolution of the first chondritic planetesimals.

INTRODUCTION

Hua and Buseck (1995) described nearly pure fayalite ($Fa_{88–100}$) grains associated with magnetite, troilite, and pentlandite in the oxidized CV3 carbonaceous chondrites of the Bali-like subgroup (Weisberg *et al.*, 1993) Kaba and Mokoia. The fayalite grains have high MnO contents (0.6–1.8 wt%); concentrations of Cr, Ca, Al, Ti, and Ni are close to the detection limits of electron microprobe analysis (EMPA) (approximately 0.04–0.07 wt%). Hua and Buseck (1995) proposed a complex multistage nebular model for the origin of fayalite. It includes oxidation of metal to magnetite at <400 K, decomposition of enstatite to SiO gas and forsterite during a reheating event above 1300 K, followed by formation of fayalite by reactions between SiO gas and magnetite or troilite at approximately 800–1200 K.

Later, Krot *et al.* (1998a,b) showed that fayalite in Kaba and Mokoia coexists with hedenbergite; fayalite and hedenbergite replace magnetite-sulfide nodules inside type-I chondrules and form veins crosscutting fine-grained chondrule rims. These authors suggested that CV fayalite and hedenbergite formed during relatively low-temperature (<300 °C) alteration in the presence of aqueous solutions in an asteroidal setting. Using ^{53}Mn-^{53}Cr chronology, Hutcheon *et al.* (1998a) estimated an age of fayalite formation in Mokoia as either 7 or 15 Ma after crystallization of Allende calcium-aluminum-rich inclusions (CAIs) and argued in favor of asteroidal formation of fayalite (two ages reported are due to the absence of a well-defined value for the solar system initial abundance of ^{53}Mn; *e.g.*, Birck and Allegre, 1988; Lugmair and Shukolyukov, 1998). Hua *et al.* (2000a) reported an even younger age of fayalite formation in Kaba (~9 or 17 Ma after Allende CAIs) but preferred high-temperature nebular setting for the origin of fayalite.

Recently, Krot and Todd (1998) described fayalite-bearing veins and fayalite–hedenbergite–magnetite–carbide assemblages in the

Bali-like clast of the reduced CV chondrite breccia Vigarano. On the basis of the petrographic observations and thermodynamic analysis, these authors argued that these assemblages resulted from asteroidal alteration. No occurrences of fayalite–hedenbergite assemblages are known in meteorites apart from the CV chondrites.

In this paper, we describe bulk chemistry, natural and induced thermoluminescence (TL), secondary minerals, and Mn- and Cr-isotopic study of fayalite from MacAlpine Hills (MAC) 88107, an ungrouped carbonaceous chondrite with bulk chemistry and mineralogy intermediate between those of CM and CO chondrites. This meteorite experienced a low degree of thermal metamorphism and very minor alteration resulting in formation of fayalite–hedenbergite–magnetite assemblages. Chondrite MAC 88107 escaped postaccretional brecciation and preserved textures that are important for understanding of mechanism of fayalite and hedenbergite formation in carbonaceous chondrites.

MacAlpine Hills 87300, 87301, and 88107 Carbonaceous Chondrites: Previous Studies

Mason (1988, 1989) described three carbonaceous chondrites from the MacAlpine Hills region of Antarctica (MAC 87300, MAC 87301, and MAC 88107) and on the basis of petrographic similarities and close proximity suggested that MAC 87300 and MAC 87301 are paired CM chondrites. Sears *et al.* (1990) showed that unlike typical CM chondrites, which have no detectable natural or induced thermoluminescence (TL), MAC 87300, MAC 87301, and MAC 88107 have both. On the basis of the similar natural TL values, Sears *et al.* (1990) suggested that these three meteorites could be paired and related to the CO3.0 chondrites, Allan Hills (ALH)A77307 and Colony.

It was later found that CAIs from MAC 87300 and MAC 88107 are mineralogically different from those in CO chondrites; in addition, the observed mineralogical differences between CAIs from MAC 88107 and MAC 87300 suggest that these meteorites are not paired (G. J. MacPherson and S. S. Russell, pers. comm., 1999).

On the basis of the Zn/Mn and Al/Mn abundance ratios, which fall in the hiatus between CM and CO chondrites, Kallemeyn (1992a,b) concluded that MAC 87300, MAC 87301, and MAC 88107 form an independent grouplet. Zolensky and coworkers (Browning *et al.*, 1991; Zolensky, 1991; Zolensky *et al.*, 1993) reported the presence of phyllosilicates in MAC 87300 and MAC 88107. Zolensky *et al.* (1993) showed that phyllosilicates in MAC 87300 consist of serpentine and saponite, with the presence of the latter in abundance clearly distinguishing this meteorite from CM chondrites. On the basis of this and other mineralogical observations, Zolensky *et al.* (1993) suggested that MAC 87300 is an ungrouped carbonaceous chondrite, most similar to Essebi.

On the basis of the presence of magnetite and absence of phyllosilicates in x-ray powder diffraction patterns and bulk O-isotopic compositions, which are similar and plot in the field of CO and CK chondrites, Clayton and Mayeda (1999) suggested that MAC 87300 and MAC 88107 belong to the CK group of meteorites.

ANALYTICAL PROCEDURES

A polished thin section of MAC 88107,50 was studied using optical microscopy, backscattered electron (BSE) imaging, x-ray elemental mapping, and electron probe microanalysis. Backscattered electron images were obtained with a Zeiss DSM-962 scanning electron microscope (SEM) using a 15 kV accelerating voltage and 1–2 nA beam current. Electron probe microanalyses were performed with a Cameca SX-50 electron microprobe using a 15 kV accelerating voltage, 10–20 nA beam current, beam size of approximately 1–2 μm, and wavelength dispersive x-ray spectroscopy. For each element, counting times on both peak and background were 30 s (10 s for Na and K). Matrix effects were corrected using PAP procedures. The x-ray elemental maps were acquired using five spectrometers of the Cameca microprobe at 15 kV accelerating voltage, 50–100 nA beam current, and approximately 1–2 μm beam size.

Demountable, doubly-polished petrographic thin sections were prepared from chips of MAC 88107 provided by the Antarctic Meteorite Working Group. The sections were mounted using Loctite 414, an epoxy which is soluble in acetone. At each stage of preparation, the sections were impregnated with epoxy to prevent disintegration during polishing. The samples were studied by optical microscopy, followed by SEM and transmission electron microscopy (TEM). This procedure allows complete characterization of the same region of the sample to be carried out at all scales. Transmission electron microscopy was carried out on a JEOL 2010 high-resolution TEM operating at 200 kV. *In situ* qualitative and quantitative analyses were obtained using an Oxford ISIS analytical system equipped with an Oxford Pentafet UTW detector. The Cliff–Lorimer thin film approximation was used for data reduction and experimental *k*-factors, determined from a variety of mineral standards, were used throughout.

Samples for instrumental neutron activation analysis (INAA) were prepared in a laminar flow hood located in a restricted-access preparation laboratory with a filtered air input to minimize contamination. The MAC 88107 specimen was received from the NASA Johnson Space Center as interior chips, with some rusty patches. The chips were cleaned with acetone and then divided into two separate samples of approximately equal mass (~320 mg each) using a stainless steel "rock-biter". These pieces were then gently crushed in an agate mortar into smaller bits that would pack well into polyethylene irradiation vials. Crushing was kept to a minimum and none of the samples were powdered. The replicate samples represent separate pieces of the original sample, not splits from a homogeneous mixture.

All INAA irradiations were performed at the UCI TRIGA reactor with a neutron flux of ~2.8×10^{12} n cm^{-2} s^{-1}. The replicate samples were irradiated in separate runs. Samples were irradiated for 2 min and counted immediately to determine elements producing very short-lived radioisotopes (Mg, Al, Ca, V, and Mn). Samples were then irradiated for 4 h in order to determine longer-lived species. They were counted several times over a period of ~6 weeks to determine elements producing longer-lived species (Na, K, Ca, Sc, Cr, Mn, Fe, Co, Ni, Zn, Ga, As, Se, Sb, rare earth elements (REE), Os, Ir, and Au). The INAA procedure is described in more detail in Kallemeyn *et al.* (1989). An Allende powder (from E. Jarosewich, N.M.N.H.) and an U.S.G.S. standard rock powder, SCo-1, were included in each run to check for possible systematic errors.

Many analyses of replicate samples of an Allende standard powder (split 13, position 4) over several years gave the following estimated relative standard deviations that are typical for the chondrite samples we run: Na, Mg, Al, Ca, Sc, V, Cr, Mn, Fe, Co, Ni, Zn, Ga, As, Se, La, Sm, Ir, and Au, 5%; and K, Sb, Ru, Eu, Yb, Lu and Os, 6–10%.

RESULTS

Bulk Chemistry

Concentrations of 27 elements in the two MAC 88107 samples are listed in Table 1. The data for both samples are very similar, generally agreeing within 10% or less. The greatest differences are

among elements most likely to be affected by weathering processes (*i.e.*, Na, K, and Ca). The CI- and Mg-normalized element abundances for lithophile and siderophile elements are plotted in Fig. 1. Elements are ordered from left to right according to decreasing nebular 50%-condensation temperature for each subgrouping. Lines representing group mean abundances for CM and CO chondrites are drawn for reference.

TABLE 1. Concentration INAA data for 27 elements in replicate samples of MAC 88107.

Element		Sample 1	Sample 2	Average
Na	mg/g	2.01	1.81	1.91
Mg	mg/g	134	132	133
Al	mg/g	13.7	13.2	13.4
K	μg/g	333	367	350
Ca	mg/g	14.4	13.6	14.0
Sc	μg/g	9.65	9.23	9.44
V	μg/g	82.2	80.1	81.2
Cr	mg/g	3.47	3.29	3.38
Mn	mg/g	1.71	1.67	1.69
Fe	mg/g	240	230	235
Co	μg/g	556	510	533
Ni	mg/g	11.1	10.1	10.6
Zn	μg/g	120	124	122
Ga	μg/g	7.7	7.5	7.6
As	μg/g	1.91	1.87	1.89
Se	μg/g	8.6	8.8	8.7
Br	μg/g	4.2	4.0	4.1
Ru	ng/g	1020	960	990
Sb	ng/g	96	109	102
La	ng/g	363	369	366
Sm	ng/g	222	226	224
Eu	ng/g	85	90	87.5
Yb	ng/g	238	256	247
Lu	ng/g	37	38	37.5
Os	ng/g	733	704	718
Ir	ng/g	688	653	670
Au	ng/g	203	181	192

The CI-normalized refractory lithophile element abundances (Al, Sc, Ca, REE, and V) for MAC 88107 are similar to those for the CM-CO clan. Moderately volatile lithophile element abundances (Cr, Mn, Na, and K), except for Na, are intermediate to those for CM and CO. The Na abundance is highly depleted relative to both CM and CO. Because the surface of the MAC 88107 meteorite has evaporite deposits (weathering index "Be"), the Na depletion is probably due to weathering effects.

Like the refractory lithophiles, refractory siderophile element abundances (Os, Ir, and Ru) are similar to those of the CM-CO clan. Common siderophile element abundances (Co, Ni, and Fe) are quite variable, unlike the flat, unfractionated pattern in a typical chondrite. The variable pattern, with Co < Ni < Fe, is typical of a weathered chondrite containing metal. Weathering results in oxidation of metal and loss of Ni and Co; the Fe abundance is the least affected because most of the Fe occurs as an oxide in silicates. We infer that the true abundances of the common siderophile elements are close to the measured Fe abundance, which is similar to those in CM and CO chondrites. Moderately volatile siderophile and chalcophile element abundances (Au, As, Ga, Sb, Br, Se, and Zn) are intermediate between CM and CO abundances. Two of the elements, Au and Br, have abundance patterns typical of CM chondrites. In the CM chondrites, the Au abundance is similar to those of the common siderophiles, not lower as is typical of CO and other carbonaceous chondrites. There is a distinctive, positive Br "anomaly" in MAC 88107 similar to that observed in CM chondrites. Because Br abundances in Antarctic meteorites can be enhanced by aerosols from sea spray transported through the atmosphere, it is possible that the Br "anomaly" is simply due to weathering and not an inherent property relating it to the CM chondrites.

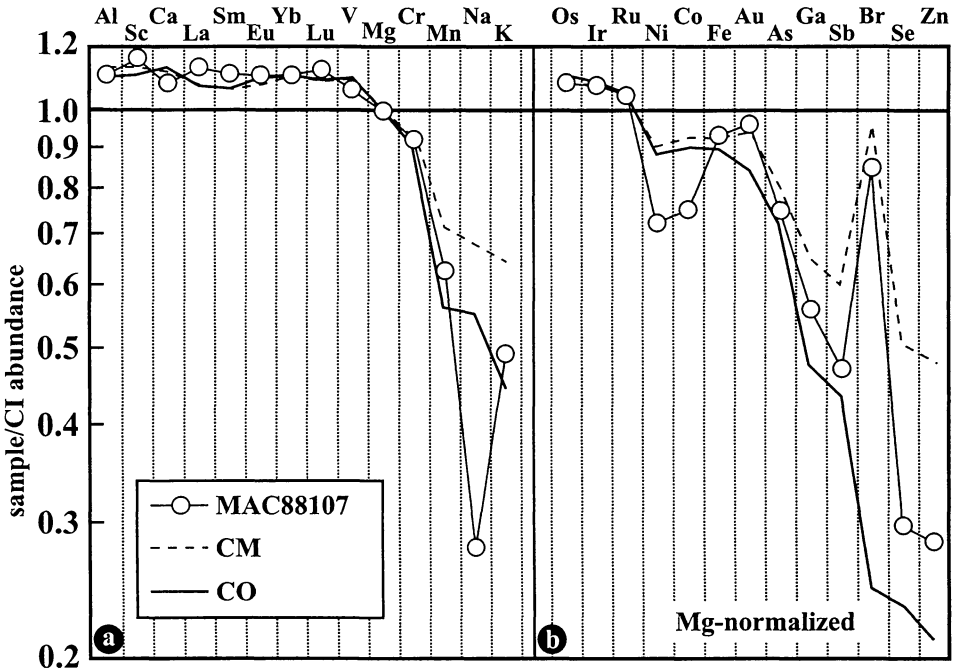

FIG. 1. The CI- and Mg-normalized abundance ratios for MAC 88107, along with mean CM and CO chondrite values (data for CM and CO chondrites from Kallemeyn and Wasson, 1982, 1985; Kallemeyn, unpubl. data). Lithophile elements are plotted in (a), and siderophile and lithophile elements are plotted in (b). Elements are arranged in order of decreasing condensation temperature.

The ratios of certain elements (*e.g.*, Zn/Mn, Al/Mn, Ga/Mg, and Sb/Mg) form distinctive clusters among the chondrite groups. The most informative of these are the Zn/Mn and Al/Mn ratios, which are generally not affected by weathering (Fig. 2). These ratios for MAC 88107 plot in a hiatus between the CM and CO clusters, although somewhat closer to CO. The Ga/Mg and Sb/Mg ratios for MAC 88107 also plot in a hiatus between the CM and CO groups (Fig. 3). Because the loss of metal from the sample must have affected both Ga and Sb, we infer that unweathered MAC 88107 would plot closer to the CM group.

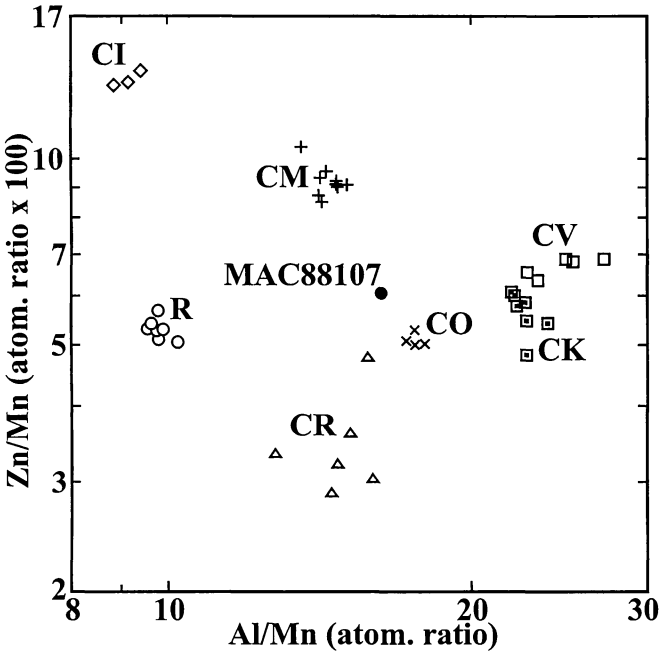

FIG. 2. Carbonaceous chondrite groups form distinct compositional clusters on a plot of Zn/Mn *vs.* Al/Mn. Chondrite MAC 88107 plots in the hiatus between CO and CM carbonaceous chondrites (data from Kallemeyn and Wasson, 1982, 1985; Kallemeyn *et al.*, 1991, 1994, 1996; Kallemeyn, unpubl. data).

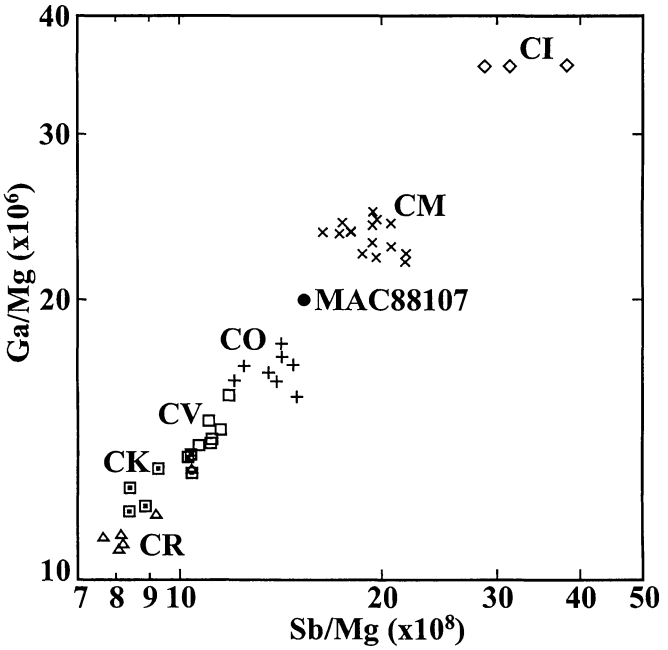

FIG. 3. Abundances of the two moderately volatile siderophile elements, Ga and Sb, show a strong correlation among the carbonaceous chondrite groups. The different chondrite groups plot in separate clusters (data from Kallemeyn and Wasson, 1982, 1985; Kallemeyn *et al.*, 1991, 1994, 1996; Kallemeyn, unpubl. data). Chondrite MAC 88107 plots in the hiatus between CO and CM carbonaceous chondrites.

The compositional data of MAC 88107 preclude its placement in the CM or CO group; it must be treated as ungrouped carbonaceous chondrite.

Natural and Induced Thermoluminescence

Meteorites MAC 87300, MAC 87301, and MAC 88107 have natural TL values of 17 ± 6, 16 ± 2, and 14 ± 1 krad (1σ uncertainties on precision), respectively. These values are on the low side of the normal range for Antarctic meteorites (values are typically 30–100 krad, but <5 and >100 krad are considered unusual), which suggests that these are meteorites with fairly large terrestrial ages (about equivalent to a period on the ice surface of ~250 000 years; Benoit *et al.*, 1993). These three meteorites have broad hummocky glow curves (plots of luminescence intensity as a function of heating temperature) similar to those of other very primitive chondrites, the Colony and ALHA77307 CO3.0 chondrites and the Lewis Cliff (LEW) 85332 CR-related meteorite, with strong emission in the 350–400 °C region (Fig. 4). Such meteorites also have distinctive cathodoluminescence properties dominated by ubiquitous fine-grained forsteritic olivine (Sears *et al.*, 1990).

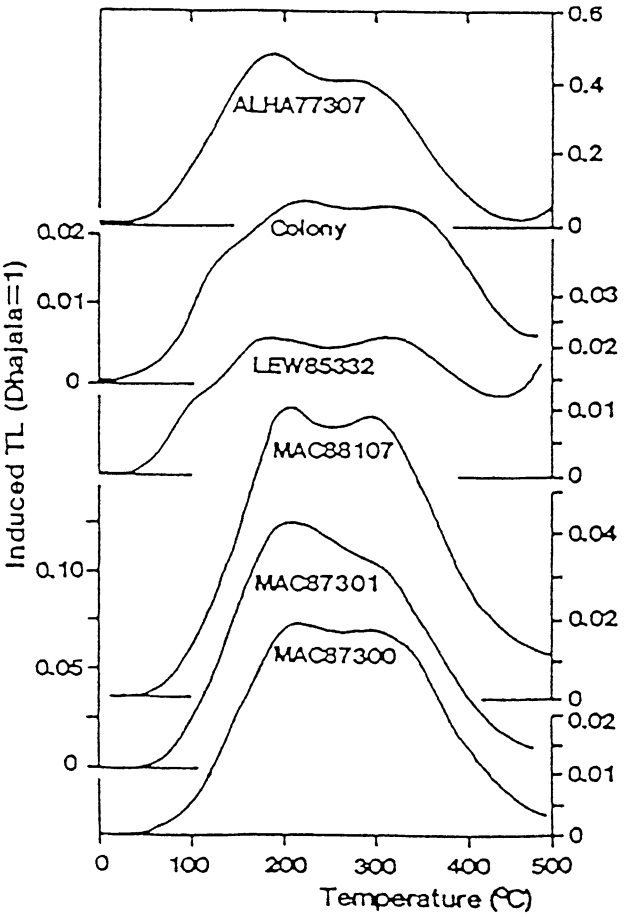

FIG. 4. Glow curves for the CO3 chondrites ALHA77307 and Colony and ungrouped carbonaceous chondrites LEW 85332, MAC 87300, MAC 87301, and MAC 88107 (from Sears *et al.*, 1990).

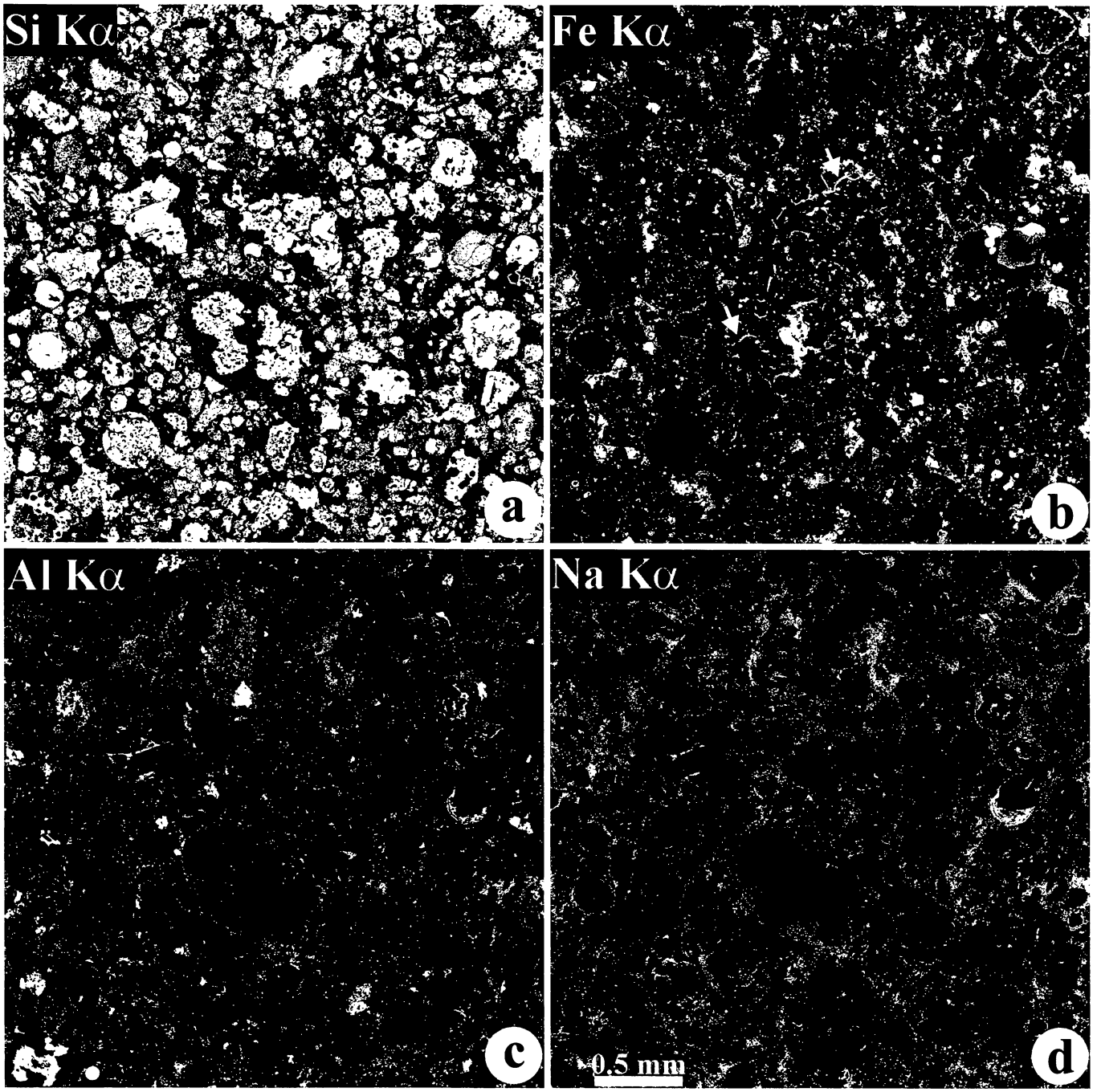

FIG. 5. X-ray elemental maps in Si (a), Fe (b), Al (c), and Na (d) of a 3 × 3 mm region of the MAC 88107 meteorite. Most coarse-grained components (CAIs, chondrules, and mineral fragments) are surrounded by continuous fine-grained rims; interstitial matrix material is virtually absent. Sodium is largely concentrated in the fine-grained rims in phyllosilicates; nepheline is absent. Several rims are crosscut by Fe-rich veins consisting of fayalite–hedenbergite–magnetite assemblages (indicated by arrows in (a) and (b)).

Unlike 21 CM chondrites run as part of the natural TL survey, which have no measurable induced TL, these three meteorites have low but significant TL sensitivities (0.012 ± 0.003, 0.03 ± 0.02, and 0.02 ± 0.01 for the metamorphism-sensitive ~120 °C peak, relative to the Dhajala standard meteorite). These values, together with Fa, suggest petrographic types of 3.0, 3.2, and 3.1 for MAC 87300, MAC 87301, and MAC 88107, respectively, where each petrographic type carries an uncertainty of 0.1 (Sears *et al.*, 1991). In fact, on a plot of TL sensitivity against olivine composition, they plot together at the low-metamorphism end of the CO chondrite trend along with Colony and ALHA77307 (Fig. 8a in Sears *et al.*, 1991).

Mineralogy and Petrography

The region of MAC 88107 exposed in the thin section studied is largely unbrecciated: most CAIs, chondrules, and isolated mineral grains are surrounded by continuous fine-grained rims; matrix material outside the rims is virtually absent (Figs. 5 and 6). These textural features are similar to the "primary accretionary textures"

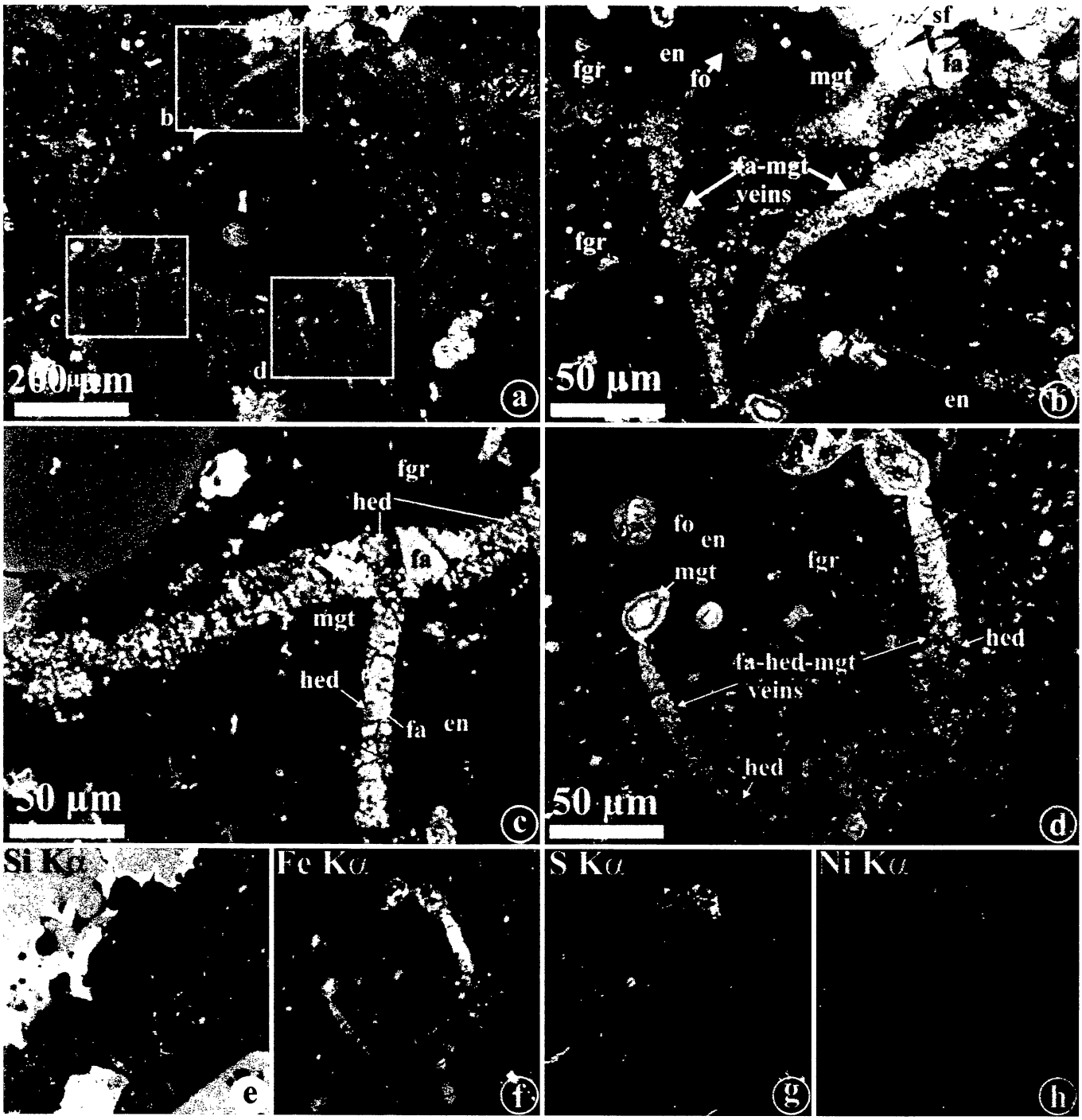

FIG. 6. Backscattered electron images (a–d, i–l) and x-ray elemental maps in Si (e), Fe (f), S (g), and Ni Kα (h) of chondrules surrounded by fine-grained rims. (a–h) Porphyritic olivine-pyroxene chondrule surrounded by a continuous fine-grained rim (fgr_1) crosscut by multiple veins. The veins consist of fayalite (fa), hedenbergite (hed), and magnetite (mgt). Outlined regions in (a) labeled as "b", "c", and "d" are shown in detail in (b), (c), and (d), respectively. Elemental maps in (e), (f), (g), and (h) correspond to a region shown in (d). Chondrule mesostasis is largely leached out, whereas forsteritic olivine (fo) and low-Ca pyroxene (en) phenocrysts appear to be unaltered (see (a) and (d)). The veins start at the opaque nodules composed of Ni-bearing sulfide and magnetite in the peripheral portion of the host chondrule and show depletion in S and Ni. Veins terminate along the boundaries with fine-grained rims around neighboring chondrules. A coarse-grained fayalite–hedenbergite–magnetite assemblage occurs between two fine-grained rims (fgr_1 and fgr_2; see (b)); its fayalite contains inclusions of magnetite suggesting that fayalite formed by replacement of magnetite.

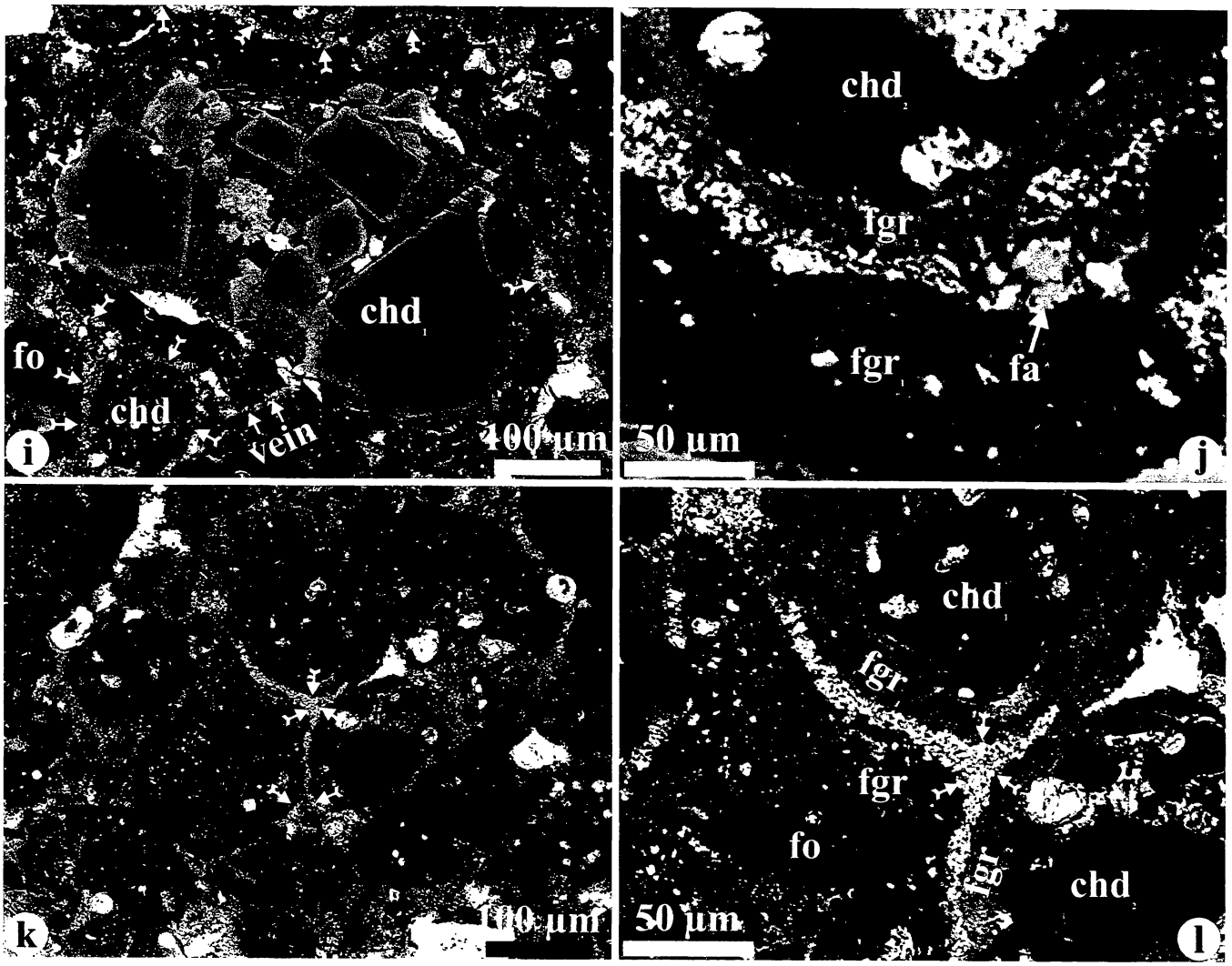

FIG. 6. *Continued.* Backscattered electron images (i–l). (i, j) Type-II chondrule (chd_1) surrounded by a fine-grained rim (fgr_1) that is crosscut by a fayalite-hedenbergite-bearing vein. The vein is connected with a fayalite-bearing layer between fine-grained rims (fgr_2) around neighboring chondrules (chd_2 and chd_3). Mesostasis of the host chondrule is largely leached out. (k, l) Fayalite-bearing layer (indicated by arrows) separating fine-grained rims (fgr_1, fgr_2, and fgr_3) around neighboring chondrules.

previously described in several CM chondrites (Metzler *et al.*, 1992; Hanowski and Brearley, 1997, 2000). Although chondrule mesostases are replaced by phyllosilicates or nearly completely leached out (Fig. 6i–l) and most of the metal-sulfide nodules are oxidized to magnetite and Ni-bearing sulfides, SEM and EPMA studies at magnifications up to 5000× showed no evidence for aqueous alteration of chondrule phenocrysts (Fig. 6). In addition to the previously described secondary minerals (phyllosilicates, magnetite, and Ni-bearing sulfides) (Browning *et al.*, 1991; Zolensky, 1991; Zolensky *et al.*, 1993), our mineralogical observations revealed the presence of abundant grains of fayalite (~Fa_{90-100}) and hedenbergite (~$Fs_{50}Wo_{50}$). These minerals are observed in several textural occurrences described in detail below.

Fayalite–Hedenbergite–Magnetite Assemblages in Fine-Grained Chondrule Rims–Fayalite–hedenbergite–magnetite assemblages in fine-grained rims around type-I (FeO-poor) and type-II (FeO-rich) chondrules occur as veins and relatively coarse-grained particles (Fig. 6). The veins commonly start at the opaque nodules in the peripheral portions of the chondrules, crosscut fine-grained rims around the host chondrules and terminate at the boundary with fine-grained rims around neighboring chondrules (Fig. 6d,i). The opaque nodules consist mainly of magnetite and Ni-bearing sulfides. X-ray elemental maps of the nodules in Ca, P, Ni, and Cr Kα also showed the presence of abundant tiny inclusions of Ca-, P-, Ni-, and Cr-rich phases, possibly Ca-phosphates, Ni-bearing sulfides, and chromite. The veins consist of fine-grained, anhedral fayalite, hedenbergite, and magnetite; Ni- and S-bearing phases are absent (Fig. 6e–h). Fayalite and hedenbergite are closely intergrown and often contain tiny inclusions of magnetite (Fig. 6b–d).

Fine-grained rims crosscut by veins typically contain nodules and irregularly-shaped coarse particles composed of fayalite, magnetite, and sulfides (Figs. 6d and 7c). Because of their small grain sizes, these minerals were identified only qualitatively using BSE and x-ray elemental maps. There is generally no preferential distribution of these particles within a rim.

One of the veins crosscuts a matrix-rich clast or an exceptionally thick fine-grained rim around an irregularly-shaped chondrule (Fig. 7). In contrast to the relatively massive, short veins that crosscut the

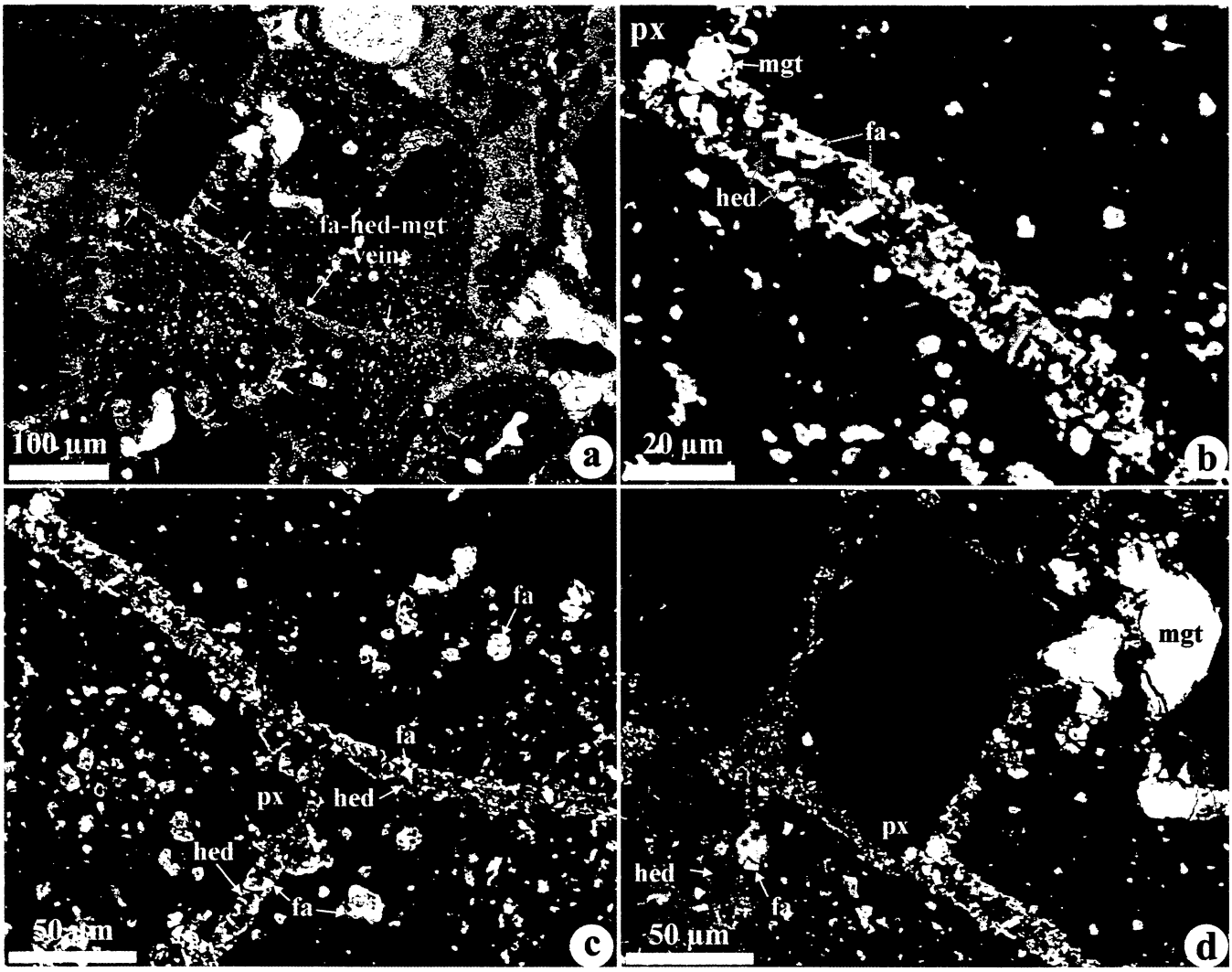

FIG. 7. Backscattered electron images of a matrix-rich clast (outlined by yellow arrows in (a)). The clast is intersected by a fayalite-hedenbergite-magnetite vein (indicated by blue arrows in (a)) that starts to the right from the clast, crosscuts it, and continues to the left as a layer between the clast and the fine-grained rims around neighboring chondrules (see (a) and (d)). The vein has a hollow central zone which is partly filled by subhedral fayalite and hedenbergite grains. Low-Ca pyroxene grains (px) in contact with the vein appear to be unaltered (see (c) and (d)).

fine-grained rims around chondrules, this vein, ~300 μm in length, consists of subhedral and euhedral grains of fayalite and hedenbergite growing towards its central hollow zone.

Fayalite–Hedenbergite–Magnetite Layers between Fine-Grained Rims–Fine-grained rims around neighboring chondrules are often separated by a discontinuous layer enriched in relatively coarse-grained fayalite and hedenbergite (Figs. 6i–l, 7a, and 8). There is a textural continuity between the veins and inter-rim layers: veins crosscutting fine-grained rims may continue as inter-rim layers (Figs. 7a and 8f).

Fayalite Overgrowing Forsteritic and Fayalitic Olivine Grains–Figure 9 illustrates several occurrences of fayalite intergrown with and overgrown onto isolated grains of forsteritic and fayalitic olivine. Some of these fayalites are part of the fayalite-hedenbergite-magnetite veins crosscutting fine-grained rims around chondrules (Fig. 9a–c), whereas for others this connection is unclear (Fig. 9d). Most of the fayalites overgrowing isolated olivine grains are observed between the fine-grained rims in the close proximity to the inter-rim fayalite-hedenbergite-bearing layers (Fig. 9e–g). These fayalites are typically coarse grained and virtually free of magnetite inclusions. The compositional profiles across the fayalite–forsteritic and fayalitic–olivine boundaries are steep; no Fe-Mg interdiffusion on the scale resolvable by EMPA (approximately 3–5 μm) has been observed (Table 2, Fig. 10).

Coarse-Grained Fayalite–Magnetite–Sulfide Assemblages–Coarse-grained fayalite–magnetite–sulfide assemblages commonly observed in the Kaba and Mokoia meteorites (Krot *et al.*, 1998a,b; Choi *et al.*, 2000) are rare in MAC 88107 (Fig. 11). Magnetite in these assemblages is nearly pure Fe_3O_4; sulfides are Ni-rich. The boundaries between fayalite and magnetite are irregular; fayalite grains contain abundant inclusions of magnetite and sulfides suggestive of the substitution of fayalite for magnetite.

Mineral Chemistry

Microprobe analyses of various textural occurrences of hedenbergite and fayalite in MAC 88107 are summarized in Table 3 and Fig. 12. Hedenbergite grains in veins and inter-rim layers are compositionally pure and contain ~0.2 wt% MnO; the concentrations

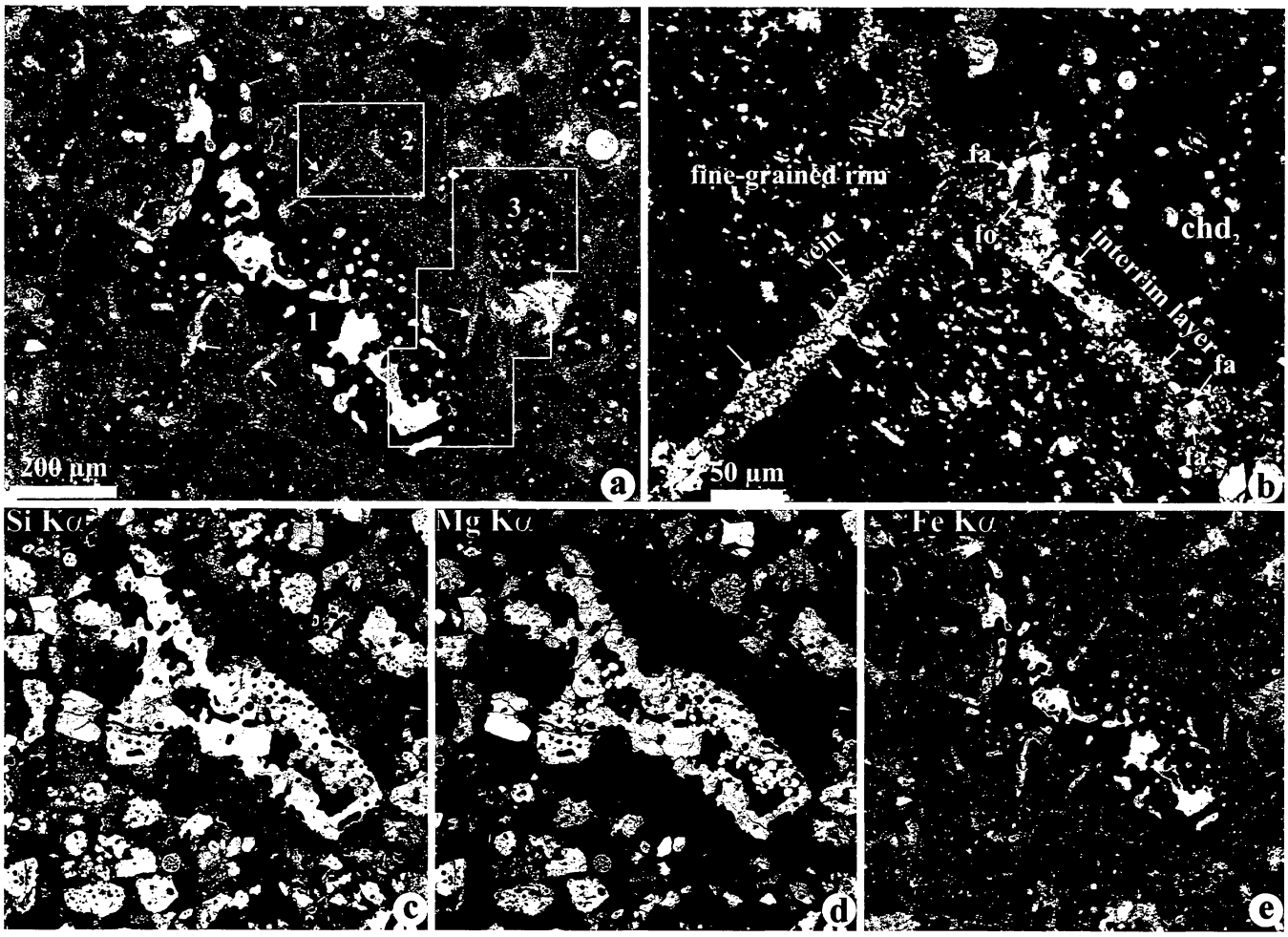

FIG. 8. Backscattered electron images (a, b, and f) and x-ray elemental maps in Si (c), Mg (d), and Fe Kα (e) of a region in MAC 88107 containing chondrules (three of them are labeled as "1", "2" and "3" in panel (a)) surrounded by the continuous fine-grained rims. (a) Fine-grained rim around the largest chondrule is crosscut by multiple fayalite-hedenbergite-magnetite veins (indicated by arrows). Outlined regions are shown in detail in (b) and (f). (b) Fayalite–hedenbergite–magnetite assemblages occur as a vein crosscutting fine-grained rim, as numerous irregularly-shaped grains concentrated in the peripheral portion of this rim, and as a discontinuous layer separating fine-grained rims around the host chondrule and a neighboring chondrule (chd_2). A fragment of forsteritic olivine close to this layer is overgrown by fayalite (fa). *Figure 8 continued on next page.*

of TiO_2, Al_2O_3, and Cr_2O_3 are close to their detection limits (approximately 0.03–0.04 wt%). There are no systematic compositional differences between the four textural varieties of fayalites described above. Most of the grains are close to endmember fayalite ($Fa_{>95}$) and have high concentrations of MnO (0.4–0.9 wt%). The apparent lower contents of the fayalite component in some of the grains ($Fa_{85–95}$) are probably due to their small sizes, which may have resulted in analytical problems during microprobe analyses (overlap of the electron probe beam with the neighboring magnesian silicates).

Transmission Electron Microscopy Study

We studied the detailed mineralogy of one fine-grained rim crosscut by fayalite-bearing veins from MAC 88107 by TEM; this rim is texturally similar to a rim shown in Fig. 6a–d. Our results are consistent with the observations of Zolensky *et al.* (1993) for MAC 87300 fine-grained material. The fine-grained rim studied was 20 to 150 μm in thickness and surrounded a porphyritic olivine-rich chondrule. The rim was crosscut in several places by veins of magnetite and fayalite, which typically extend from the opaque nodules on the periphery of the chondrule to the outside of the rim. Low-magnification TEM images of the rim material show that it is extremely fine-grained in character (only a few crystalline grains are >200 nm in size) and has a complex microstructure (Fig. 13a). The rim material is characterized by Fe-rich phases that appear dark in the image, embedded in a groundmass of material with lower contrast.

Detailed studies of the low contrast material show that it is dominated by a material that ranges from amorphous to nanocrystalline in character (Figs. 13b and 14a). In many regions of the rim, this material has a distinct porous appearance (Fig. 14a) that does not appear to be the result of beam damage. The degree of crystallinity of this material is extremely low, as indicated by electron diffraction patterns that have broad, diffuse rings characteristic of an amorphous or poorly ordered material. High-resolution TEM studies show that this material has partially recrystallized to form myriad, nanocrystalline phyllosilicate crystals that are probably best described as protophyllosilicates. These crystallites are up to ~15 nm in length and two to seven unit cells in thickness (Fig. 14b). They typically have curved lattice fringes and a range of basal spacings. Most crystallites have basal lattice

FIG. 8. *Continued.* (f) A continuous fayalite-hedenbergite-magnetite layer separating fine-grained rims (frg_1 and fgr_3) around two neighboring chondrules (chd_1 and chd_3).

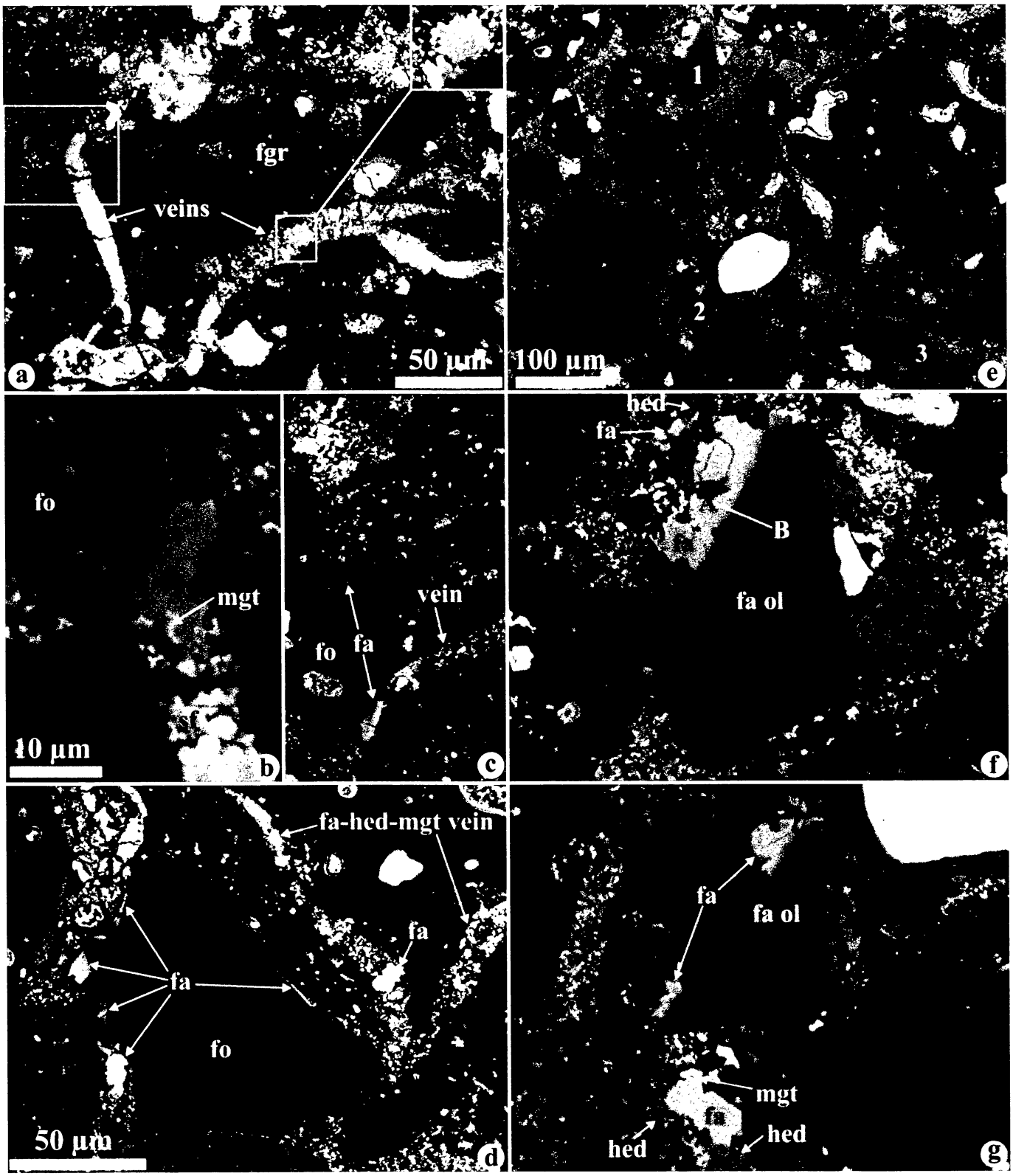

FIG. 9. Backscattered electron images of fayalitic and forsteritic olivine grains overgrown by fayalite in MAC 88107. (a–c) Fayalites (fa) of the veins crosscutting fine-grained rims (fgr) around chondrules are intergrown with forsterite grains (fo). (d) Forsterite grain near a fayalite-hedenbergite-magnetite vein is overgrown by fayalite. (e–g) Two fayalitic olivine (fa ol) grains (labeled as "1" and "2" in panel (e)) and a forsteritic olivine (fo) grain (labeled as "3" in panel (e)) are overgrown by fayalite. Label AB in (f) indicates compositional profile across fayalite–fayalitic-olivine boundary shown in Fig. 10.

TABLE 2. Microprobe analyses of the intergrown fayalites and forsteritic–fayalitic olivines.

							Profiles across forsteritic and fayalitic olivine–fayalite boundaries													
Mineral (d, μm)	fo*	fa*	fo	fa	fo†	fa†	fo 0	fo 3	fo 6	fo 9	fo 12	fo 15	fa 18	fa 21	fo‡ 0	fo 3	fo 6	fo 9	fo 12	fa 15	fa 18
SiO_2	42.6	29.9	42.0	29.0	36.7	28.8	42.3	42.4	42.4	42.3	42.0	41.8	28.8	28.8	35.7	35.7	36.0	35.5	32.9	29.4	28.8
TiO_2	0.07	<0.03	0.05	<0.03	<0.03	<0.03	0.04	<0.03	<0.03	<0.03	<0.03	<0.03	<0.03	<0.03	<0.03	<0.03	<0.03	<0.03	<0.03	<0.03	<0.03
Al_2O_3	0.20	<0.03	0.15	<0.03	0.13	<0.03	<0.03	<0.03	<0.03	<0.03	0.04	0.05	<0.03	<0.03	0.04	0.06	0.05	0.05	<0.03	<0.03	<0.03
Cr_2O_3	0.16	<0.03	0.43	0.05	0.41	0.05	0.17	0.18	0.15	0.14	0.18	0.30	<0.03	<0.03	0.18	0.18	0.10	0.09	0.23	0.06	<0.03
FeO	0.64	67.1	1.3	68.0	27.1	68.7	0.73	0.74	0.79	0.90	0.96	1.1	67.5	69.0	33.1	32.5	32.0	33.5	48.9	65.9	68.5
MnO	<0.04	0.87	<0.04	0.71	0.28	0.74	<0.04	<0.04	<0.04	<0.04	<0.04	<0.04	0.81	0.67	0.40	0.41	0.38	0.34	0.47	0.64	0.66
MgO	56.6	1.4	56.3	0.16	34.1	0.12	56.8	57.0	57.0	56.9	56.9	56.9	0.25	0.20	29.7	30.4	31.0	29.8	16.2	2.6	0.40
CaO	0.48	0.14	0.32	0.06	0.36	0.17	0.14	0.12	0.11	0.13	0.13	0.11	0.16	0.18	0.29	0.26	0.24	0.20	0.11	0.07	0.06
Total	100.8	99.5	100.6	98.0	99.1	98.6	100.2	100.5	100.5	100.3	100.3	100.3	97.6	98.9	99.4	99.5	99.8	99.4	98.8	98.7	98.4
Fa	0.6	96.3	1.3	99.6	30.8	99.7	0.7	0.7	0.8	0.9	0.9	1.0	99.3	99.5	38.5	37.5	36.7	38.7	62.9	93.3	99.0
							Cation formula based on four O														
Si	1.00	1.00	0.99	1.00	0.99	0.99	0.99	0.99	0.99	0.99	0.99	0.98	1.00	0.99	0.99	0.99	0.99	0.98	1.00	0.99	0.99
Ti	0.001	–	0.001	–	–	–	0.001	–	–	–	–	–	–	–	–	–	–	–	–	–	–
Al	0.005	–	0.004	–	0.004	–	–	–	–	–	0.001	0.001	–	–	0.001	0.002	0.002	0.002	0.001	–	–
Cr	0.003	–	0.008	0.001	0.009	0.001	0.003	0.003	0.003	0.003	0.003	0.006	–	–	0.004	0.004	0.002	0.002	0.005	0.002	–
Fe	0.01	1.89	0.03	1.96	0.61	1.98	0.01	0.01	0.02	0.02	0.02	0.02	1.96	1.98	0.77	0.75	0.74	0.78	1.24	1.86	1.97
Mn	–	0.025	–	0.021	0.006	0.022	–	–	–	–	–	–	0.024	0.020	0.009	0.010	0.009	0.008	0.012	0.018	0.019
Mg	1.97	0.07	1.97	0.01	1.37	0.01	1.99	1.99	1.99	1.99	1.99	2.00	0.01	0.01	1.23	1.25	1.27	1.23	0.73	0.13	0.02
Ca	0.012	0.005	0.008	0.002	0.010	0.006	0.003	0.003	0.003	0.003	0.003	0.003	0.006	0.006	0.009	0.008	0.007	0.006	0.004	0.003	0.002
Total	3.00	2.99	3.00	3.00	3.00	3.01	3.00	3.00	3.00	3.01	3.01	3.01	3.00	3.01	3.01	3.01	3.01	3.01	3.00	3.01	3.01

*Fayalite (fa) intergrown with forsterite (fo) is shown in Fig. 9a.
†Fayalite intergrown with FeO-rich olivine is shown in Fig. 9g.
‡Profile AB (Fig. 9f).

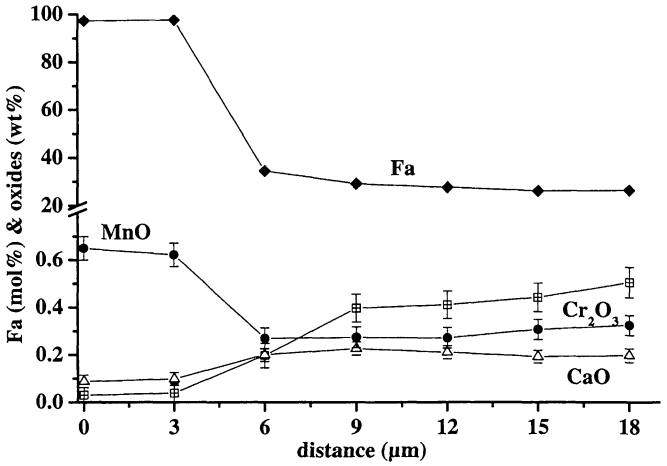

FIG. 10. Compositional profile (labeled as "AB" in Fig. 9b) across fayalite–fayalitic-olivine boundary.

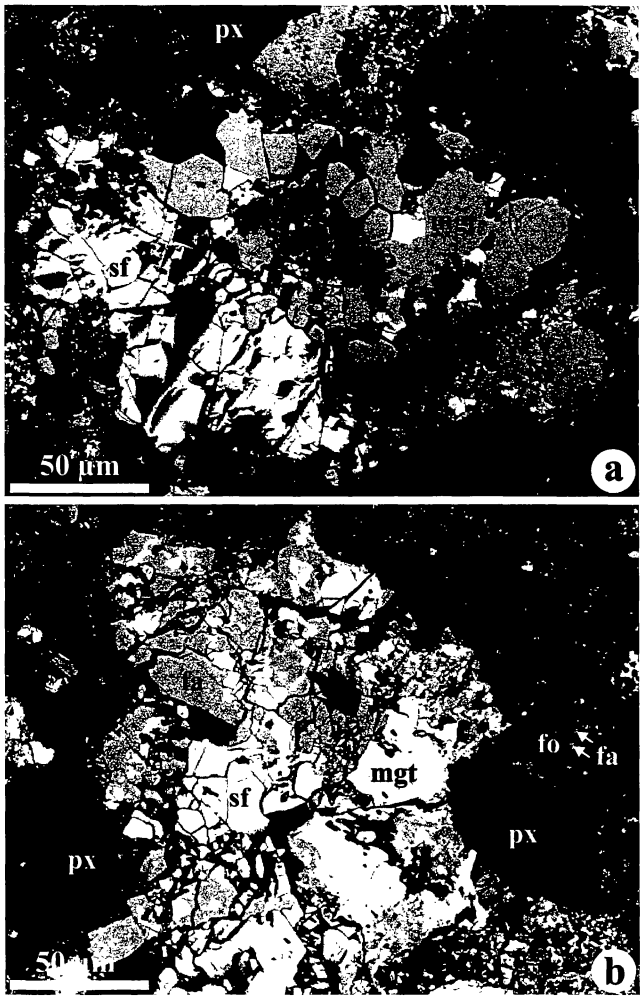

FIG. 11. Backscattered electron images of the coarse-grained fayalite–magnetite–sulfide assemblages in MAC 88107. The boundaries between fayalite (fa) and magnetite (mgt) are very irregular; fayalite contains abundant inclusions of magnetite and Ni-bearing sulfide (sf). Low-Ca pyroxene grains (px) at the contact with fayalite and magnetite (see (b)) and forsteritic olivine grain (fo) overgrown by fayalite (see (b)) appear to be unaltered.

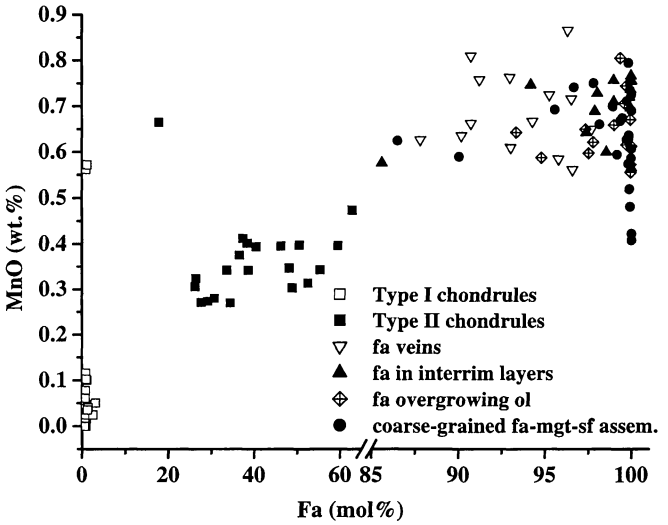

FIG. 12. Compositions of the forsteritic and fayalitic olivine phenocrysts in type-I and type-II chondrules and fayalite in different textural occurrences: veins, inter-rim layers, intergrowths with forsteritic and fayalitic olivine grains, and coarse-grained fayalite–magnetite–sulfide assemblages.

spacings of ~1.1 nm up to ~1.35 nm suggesting that they may be a smectite (probably saponite) that has suffered collapse of the interlayer site in vacuum of the TEM. Basal spacings of ~0.7 nm also occur suggesting that a serpentine-like phase may also be present. This conclusion appears to be supported by the fact that some of the larger grains have a highly curved morphology and crystals that are almost circular also occur, a feature that is commonly observed in serpentines in CM chondrites (*e.g.*, Akai, 1982; Brearley, 1995). Even though the crystallites of serpentine and smectite are extremely small, there is evidence that coherent intergrowths of the two phases occur (Fig. 14b).

A number of other additional phases also occur within the amorphous and microcrystalline groundmass. Occasionally, distinct, larger crystallites of phyllosilicates are found. They are not especially abundant and appear to occur locally in groups. Figure 13b shows an image of a region of the rim that contains several highly elongate, platy crystals of the phyllosilicate phases. The crystallites occur in random orientations, set within the amorphous groundmass and range from 0.05 to 0.25 μm in length and <26 nm in width. In other regions, there appear to be some phyllosilicates that are intermediate in size between these coarse-grained phyllosilicates and the microcrystalline phases discussed above. These crystallites are dominantly saponite crystallites with basal spacings between 1.1 and 1.4 nm that occur in small clusters in the matrix (Fig. 15a) and are up to 10 nm in width and several tens of nanometers in length.

Other crystalline silicate phases are relatively rare in the fine-grained rim. A few grains of essentially pure forsterite were found. These grains have a grain size between 0.5 and 1 μm. Irregularly-shaped, more fayalitic olivine grains have also been observed, distributed within the amorphous and microcrystalline groundmass. Some Mg-rich, low-Ca pyroxene grains are also present that are disordered intergrowths of ortho- and clinopyroxene. The grains are elongate (up to ~1.4 μm in length) and appear to be fragments, probably produced by the contraction that occurs parallel to the *c*-axis during the protopyroxene to clinopyroxene during cooling.

Magnetite is a common phase in the rim material. It occurs as anhedral to subhedral grains that can occur in clusters (Fig. 15b) and

TABLE 3. Microprobe analyses of fayalite and hedenbergite from MAC 88107.

Mineral	hed vein	hed layer	fa vein	fa vein	fa layer	fa layer	fa rim	fa rim	fa fa-mgt-sf ass.	fa fa-mgt-sf ass.
SiO_2	47.5	47.2	29.1	29.5	28.9	28.8	28.9	29.1	29.4	29.0
TiO_2	<0.04	<0.04	<0.04	<0.04	<0.04	<0.04	<0.04	<0.04	<0.04	<0.04
Al_2O_3	0.04	<0.03	<0.03	<0.03	<0.03	<0.03	<0.03	<0.03	<0.03	<0.03
Cr_2O_3	<0.03	<0.03	<0.03	<0.03	<0.03	<0.03	0.06	<0.03	<0.03	0.05
FeO	28.1	29.1	67.1	67.5	68.9	68.5	69.0	68.5	67.8	69.0
MnO	0.22	0.25	0.65	0.56	0.75	0.77	0.62	0.56	0.75	0.79
MgO	0.48	0.07	0.89	1.3	<0.03	<0.03	0.11	<0.03	0.85	0.07
CaO	22.2	21.8	0.22	0.13	0.14	0.34	0.10	0.17	0.16	0.07
Na_2O	<0.05	<0.05	<0.05	<0.05	<0.05	<0.05	<0.05	<0.05	<0.05	<0.05
K_2O	<0.04	<0.04	<0.04	<0.04	<0.04	<0.04	<0.04	<0.04	<0.04	<0.04
Total	98.5	98.5	98.0	99.0	98.8	98.5	98.7	98.4	99.1	99.0
Fa	–	–	97.7	96.6	100	100	99.7	100	97.8	99.8
Fs	49.0	50.9	–	–	–	–	–	–	–	–
Wo	49.5	48.9	–	–	–	–	–	–	–	–
					Cation formula based on					
	6 O	6 O	4 O	4 O	4 O	4 O	4 O	4 O	4 O	4 O
Si	1.99	1.99	1.00	1.00	0.99	0.99	0.99	1.00	1.00	0.99
Ti	–	–	–	–	–	–	–	–	–	–
Al	0.002	–	–	–	–	–	–	–	–	–
Cr	–	–	–	–	–	–	0.001	–	–	0.010
Fe	0.98	1.02	1.93	1.91	1.98	1.97	1.98	1.97	1.93	1.98
Mn	0.008	0.009	0.019	0.016	0.022	0.022	0.018	0.016	0.022	0.023
Mg	0.030	0.005	0.046	0.067	–	–	0.006	–	0.043	0.003
Ca	0.996	0.985	0.008	0.005	0.005	0.013	0.004	0.006	0.006	0.003
Na	–	–	–	–	–	–	–	–	–	–
K	–	–	–	–	–	–	–	–	–	–
Total	4.01	4.01	3.00	3.00	3.00	3.00	3.00	2.99	3.00	3.01

Abbreviations: hed = hedenbergite; fa = fayalite; vein = veins crosscutting fine-grained rims; layer = inter-rim layers; rim = overgrowths and intergrowths with olivine; fa-mgt-sf ass. = coarse-grained fayalite–magnetite–fayalite assemblages.

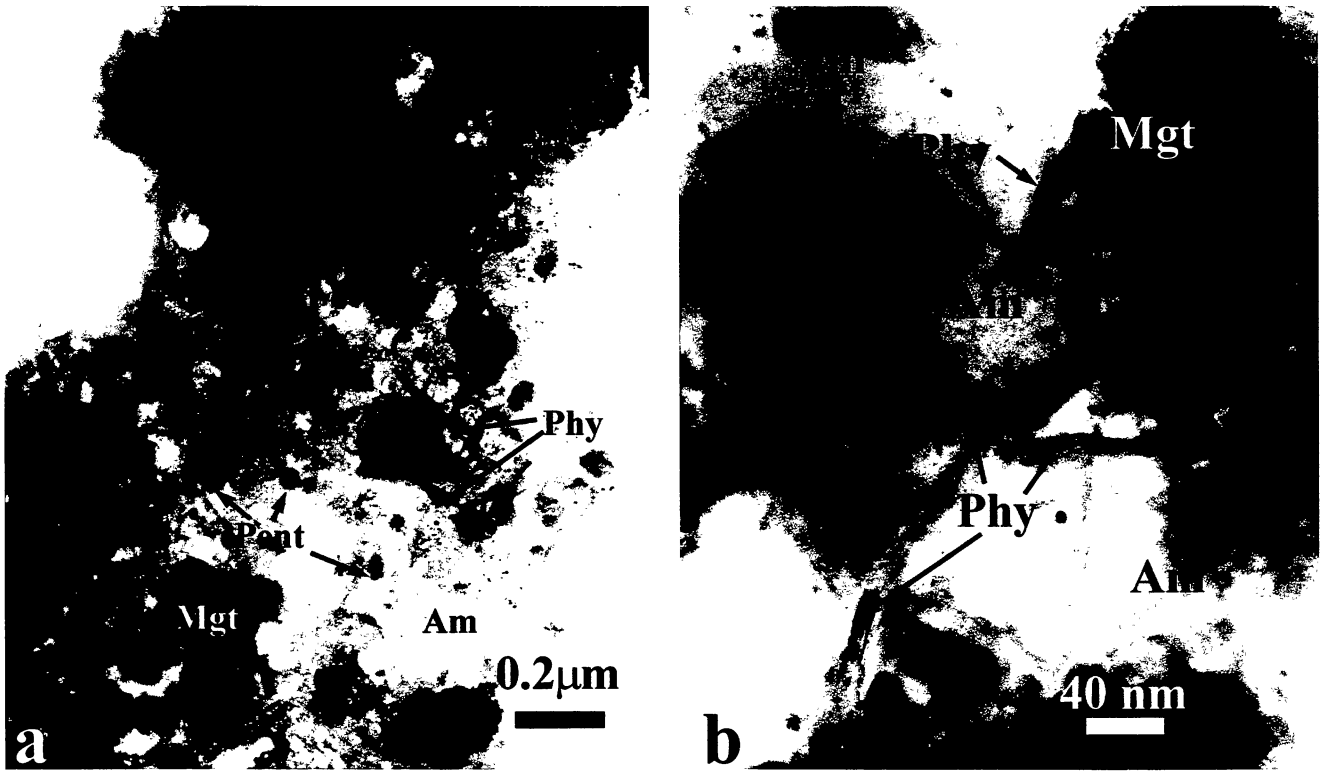

FIG. 13. Bright-field TEM micrographs of the microstructures present in a fine-grained rim around chondrule from MAC 88107. (a) The rim consists predominantly of amorphous and microcrystalline material (Am) that acts as a groundmass to coarser-grained crystalline phases, such as magnetite (Mgt), sulfides (pentlandite, Pent), and phyllosilicates (Phy). (b) Higher magnification image of the rim showing well-crystallized, elongate phyllosilicate crystals, embedded within the amorphous and microcrystalline material.

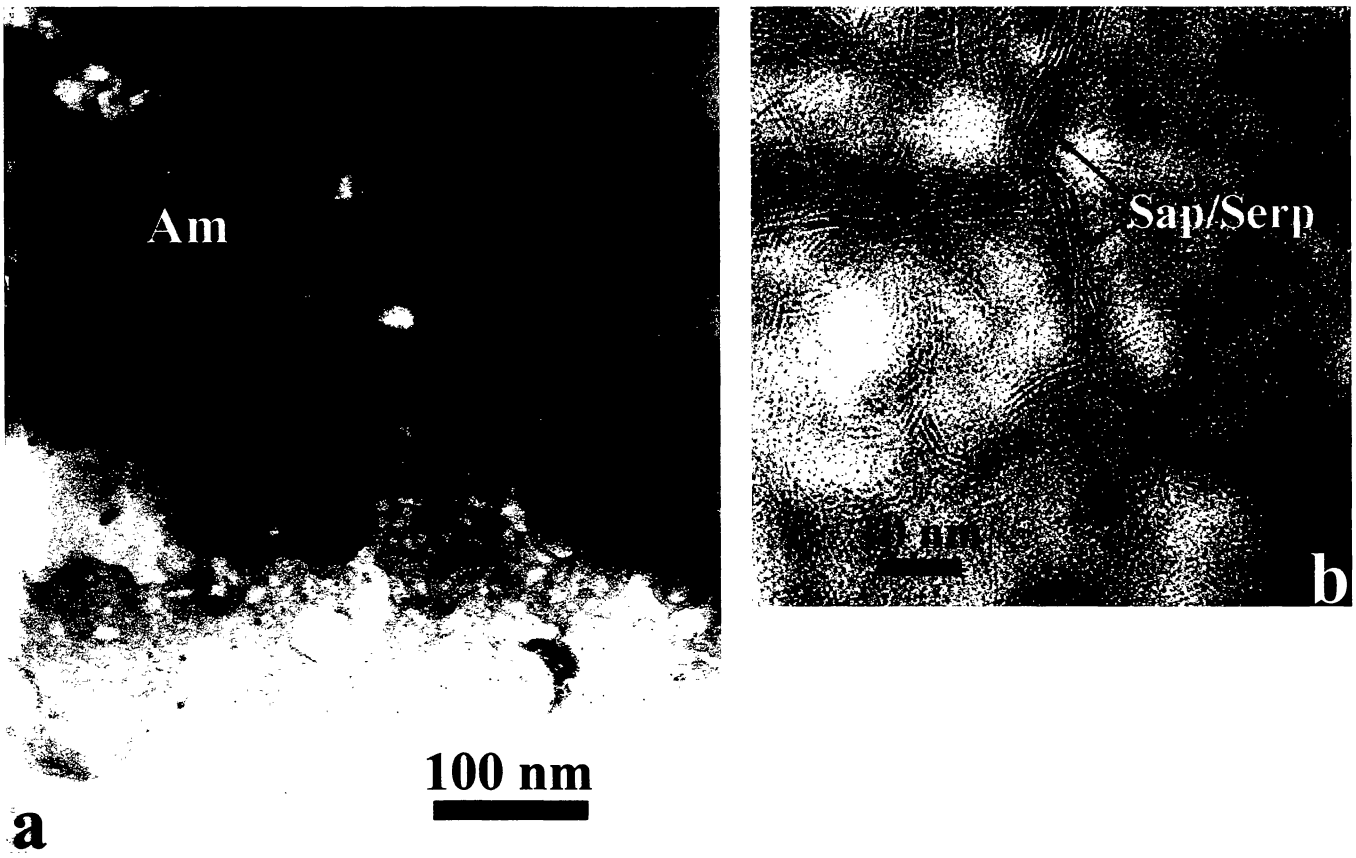

FIG. 14. (a) Bright-field TEM image of a region of amorphous and microcrystalline material (Am) in a rim region of MAC 88107. The amorphous material has a porous appearance that does not appear to be the result of electron beam damage. (b) High-resolution TEM image of the amorphous material showing that nanocrystalline phyllosilicate phases are commonly present. The crystallites show a low degree of crystallinity and appear to consists typically of intergrown smectite, probably saponite (Sap) and serpentine (Serp).

as isolated crystals. The isolated grains range typically from 20 to 50 nm in diameter, although rare larger grains also occur. The clusters of magnetite grains have irregular shapes but can be up to 0.75 μm in the longest dimension. Each cluster is made up of anhedral to subhedral grains which vary from 10 to 200 nm in size.

Two sulfide phases, pentlandite and pyrrhotite, occur in the rim studied. Both phases occur distributed throughout the amorphous and microcrystalline groundmass. Of these two, pentlandite appears to be the most abundant, invariably occurring as anhedral to subrounded grains that are invariably <200 nm in size and can be as small as 30 nm. The pyrrhotite grains are less abundant but have a similar size range to the pentlandite. In common with other occurrences of in chondrites matrices, pyrrhotite in MAC 88107 is Ni-bearing, with Ni concentrations up to ~4 wt%.

Manganese- and Chromium-Isotopic Systematics

Most fayalite grains in MAC 88107 are too small (<10 μm) for Mn- and Cr-isotopic study by an ion microprobe; as a result, no isotope measurements were done on fayalite in fine-grained rims and in layers between fine-grained rims. Because only two coarse-grained fayalite–magnetite assemblages were found in the thin section of MAC 88107,50 studied, we decided to analyze Cr isotopes in fayalite of one of them and to keep another assemblage for future O-isotopic study of the coexisting fayalite and magnetite.

The Cr-isotopic compositions of two regions of one fayalite crystal (Fig. 11b) and adjacent matrix in MAC 88107 were determined with the LLNL ion microprobe, using the procedures and standards described in Hutcheon *et al.* (1998a). Both analyses of the fayalite grain show large excesses of ^{53}Cr, ranging up to ~870‰, which are linearly correlated with the respective ^{55}Mn/^{52}Cr ratios (Table 4). The linear correlation between the magnitudes of the ^{53}Cr excesses and the respective Mn/Cr ratios is characteristic of the *in situ* decay of ^{53}Mn and demonstrates that this fayalite crystal formed while ^{53}Mn was still extant. The slope of the correlation line fitted to the data (Fig. 16), passing through the normal Cr-isotopic composition of matrix (δ^{53}Cr = 0) at Mn/Cr $\cong$ 1, indicates an initial abundance of ^{53}Mn corresponding to ^{53}Mn/^{55}Mn = (1.58 $\pm$ 0.26) $\times$ 10^{-6} at the time the fayalites formed and cooled below the closure temperature for Mn and Cr diffusion. We note that additional Mn- and Cr-isotopic measurements of fayalite in MAC 88107 are required to get a more reliable correlation line.

DISCUSSION

Fayalite and magnetite can coexist in a wide temperature range (*e.g.*, well-known QFM buffer); therefore, the key issue of the origin of fayalite in carbonaceous chondrites (Kaba, Mokoia, and MAC 88107) is not the temperature or redox conditions of the fayalite formation, but the mechanism of Si, Mn (and Fe, if fayalite formed by precipitation from a fluid) transport. The nebular model (Hua and Buseck, 1995) of fayalite formation invokes a high-temperature gas as a transportive medium, whereas the asteroidal model (Krot *et al.*, 1998a,b) invokes low-temperature aqueous solutions to transport Si,

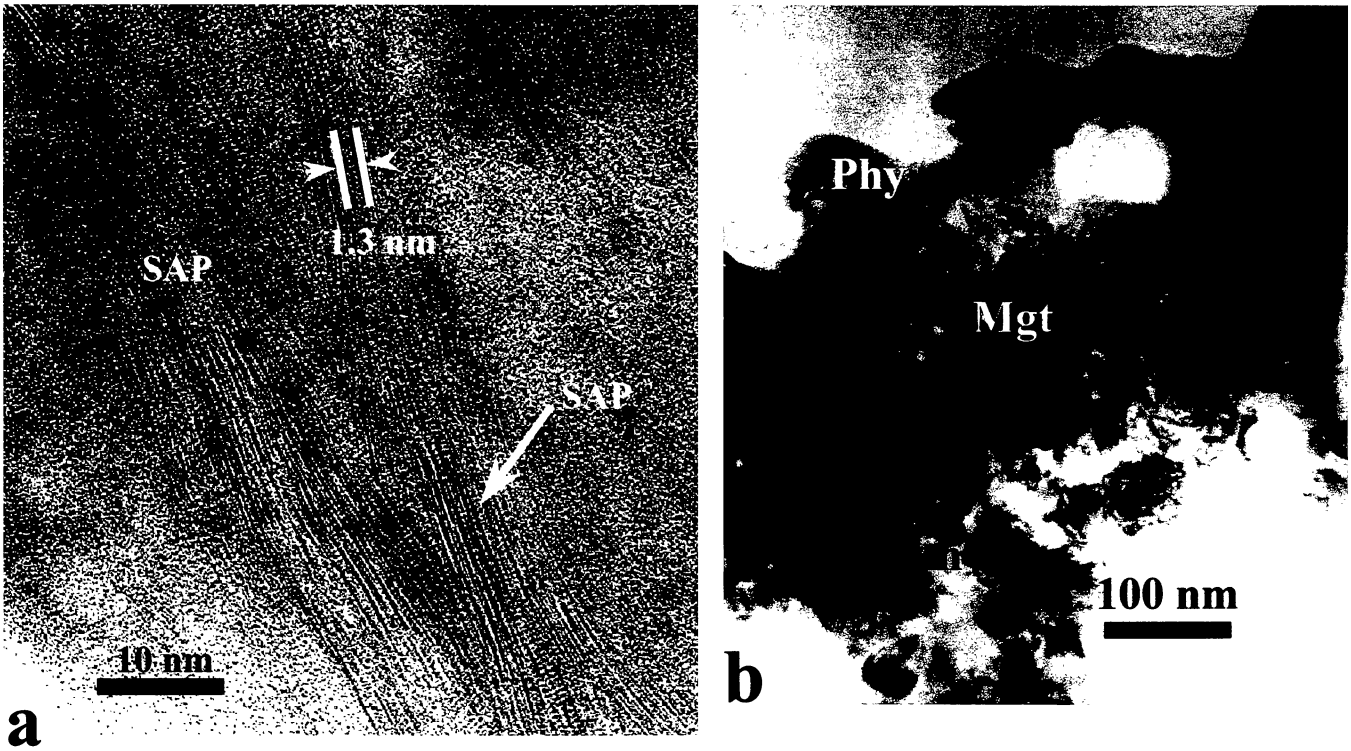

FIG. 15. (a) High-resolution TEM image of an occurrence of relatively well-crystallized, somewhat coarser-grained phyllosilicate crystals such as those shown in Fig. 14b. The crystals occur in clusters of subparallel elongate crystals with basal spacings of 1.1 to 1.4 nm that is consistent with a smectite (saponite). (b) Bright-field TEM image of a irregularly-shaped magnetite (Mgt) crystals that occur commonly within the fine-grained rim, associated with phyllosilicates (Phy) and amorphous material (Am). The grains are closely intergrown but have anhedral morphologies with little or no evidence of facets.

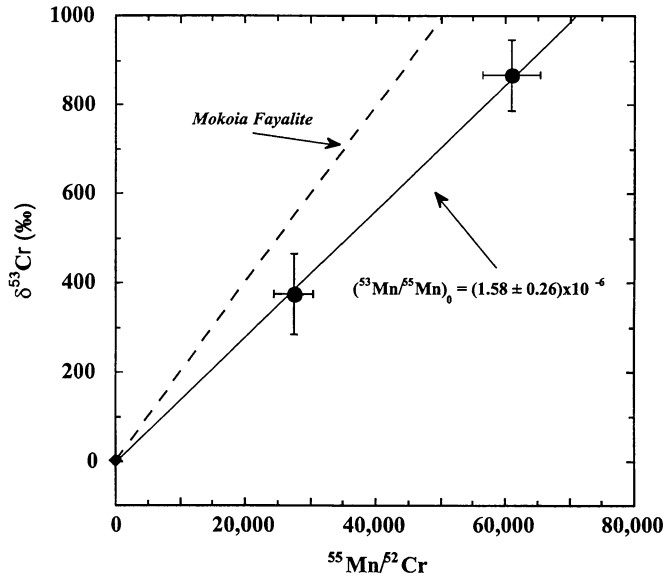

FIG. 16. Evolution diagram of ^{53}Mn-^{53}Cr for fayalite grains shown in Fig. 11b. The data are plotted as $\delta^{53}Cr$, the per mil deviation of the measured $^{53}Cr/^{52}Cr$ from the value measured in a fayalite standard; uncertainties are 2σ. The correlation line defined by data from Mokoia fayalite, slope corresponding to $^{53}Mn/^{55}Mn = (2.32 \pm 0.18) \times 10^{-6}$, is shown for comparison (data from Hutcheon *et al.*, 1998a).

Mn, Fe, and Ca. In the following section, we present arguments against the high-temperature nebular model of Hua and Buseck (1995). An asteroidal setting of fayalite and hedenbergite formation is discussed in detail by Krot *et al.* (1998a,b) and in the following sections entitled Evidence for Growth of Fayalite and Hedenbergite in MacAlpine Hills 88107 during Low-Temperature Aqueous Alteration and Physico–Chemical Conditions of Alteration.

TABLE 4. Manganese- and chromium-isotopic analysis of fayalite from MAC 88107.

Sample	$^{53}Mn/^{53}Cr$	2σ	$\delta^{53}Cr$ (‰)	2σ (‰)
Matrix	1.2	0.2	2.7	2.0
$Fa_{18\text{-}1}$	27 500	3000	376	90
$Fa_{18\text{-}2}$	61 000	4500	867	82

Arguments against High-Temperature Origin of Fayalite and Hedenbergite

According to the nebular model of Hua and Buseck (1995), fayalite formed by reactions of gaseous SiO, produced by decomposition of enstatite (reaction (1)), and solid magnetite and troilite (reactions (2) and (3)):

$$2\ MgSiO_{3(s)} + H_{2(g)} = Mg_2SiO_{4(s)} + SiO_{(g)} + H_2O_{(g)} \quad (1)$$

$$2\ Fe_3O_{4(s)} + 3\ SiO_{(g)} + H_2O_{(g)} = 3\ Fe_2SiO_{4(s)} + H_{2(g)} \quad (2)$$

$$2\ FeS_{(s)} + SiO_{(g)} + 3\ H_2O_{(g)} = Fe_2SiO_{4(s)} + H_{2(g)} + 2\ H_2S_{(g)} \quad (3)$$

Their thermodynamic analysis of *P–T–X* conditions of the reactions (1–3) predicts stable coexistence of fayalite, magnetite, and troilite below 1200 K in a gas with an H_2O/H_2 ratios of approximately 0.01–10, which is several orders of magnitude higher than the canonical solar nebula value of $\sim 7 \times 10^{-4}$ (*e.g.*, Wasson and Krot, 1994). Recently, Hua *et al.* (2000b) argued that vaporization of Si occurred during chondrule formation from chondrule melts.

Below, we discuss mineralogical, chemical, and thermodynamic arguments against the high-temperature formation of fayalite (and hedenbergite) in Kaba, Mokoia, and MAC 88107.

Mineralogical and Chemical Arguments–Hua and Buseck (1995) noted that "Kaba and Mokoia contain a wide range of chondrule types, and fayalite occurs in all of them…". Krot *et al.* (1998a,b) and Choi *et al.* (2000) confirmed these observations and described fayalite replacing magnetite nodules inside type-I chondrules containing igneous mesostasis (*e.g.*, Figs. 1 and 2 in Choi *et al.*, 2000). Hua and Buseck (1995) inferred that "it appears likely that the fayalite formed at high temperatures, where reaction rates with coexisting forsterite would have been appreciable, and had they been near each other, the forsterite and fayalite would surely have reacted. The lack of compositional gradients indicates that the two phases only came together after they cooled…". On the basis of these observations, one has to conclude that igneous textures of fayalite-bearing chondrules formed at very low temperatures. This explanation is inconsistent with high liquidus temperatures of chondrules, which are in the range of 1350–1800 °C (Scott *et al.*, 1996).

If fayalite formed at high temperatures by replacement of magnetite nodules inside type-I chondrules, then fayalite would inevitably exchange Fe with chondrule forsterite. Therefore, the lack of compositional gradients in adjacent fayalite and forsterite grains inside chondrules must be interpreted as unambiguous evidence for the formation of fayalite at temperatures low enough to prevent diffusional exchange of Fe and Mg between fayalite and forsterite. For example, at temperatures below 150 °C the exchange of Fe and Mg in an olivine grain on a scale of 5 μm would take more than 4.5 Ga (Petaev and Brearley, 1994).

Petrographic observations of Krot *et al.* (1998a,b; this study) and Choi *et al.* (2000) show that fayalite in Kaba, Mokoia, and MAC 88107 coexists with hedenbergite. Both minerals occur inside type-I chondrules in Kaba and Mokoia (see Fig. 1 in Choi *et al.*, 2000) and as veins crosscutting fine-grained rims around chondrules (see Fig. 4 in Choi *et al.*, 2000; Fig. 6). On the basis of these observations, we infer that fayalite and hedenbergite formed during the same alteration process; this process postdated chondrule formation, accretion, and compaction of fine-grained chondrule rims. Because Ca is a very refractory lithophile element (*e.g.*, Larimer and Wasson, 1988), high-temperature formation of hedenbergite by gas–solid reactions must have resulted in melting and vaporization of the fine-grained chondrule rims that are crosscut by hedenbergite-bearing veins. However, no mineralogical evidence for this high-temperature processing of fine-grained rims has been observed. Moreover, it is generally believed that fine-grained chondrule rims in primitive meteorites (petrologic types of 3.0–3.2) never experienced heating above 300 °C (Scott *et al.*, 1988; Brearley, 1996).

The condensation origin of hedenbergite coexisting with fayalite is also inconsistent with its Al-free composition. Calcium and Al are refractory lithophile elements of similar volatility and cannot be fractionated during high-temperature processing, evaporation, and recondensation (Hashimoto, 1992). In contrast, this fractionation is commonly observed in minerals produced during low-temperature aqueous alteration (*e.g.*, carbonates) (see also Evidence for Growth of Fayalite and Hedenbergite in MacAlpine Hills 88107 during Low-Temperature Aqueous Alteration).

We infer that mineralogy and chemistry of fayalite-bearing assemblages in MAC 88107, Kaba, and Mokoia are inconsistent with their high-temperature formation required by the model of Hua and Buseck (1995).

Thermodynamic Arguments–In the thermodynamic analysis of nebular *P–T–X* conditions favorable for fayalite formation, Hua and Buseck (1995) assumed that the fayalite formed in an idealized system that includes only three gaseous (H_2O, H_2, and SiO) and three condensed (Fe_3O_4, $Mg_2Si_2O_6$, and Mg_2SiO_4) species. Obviously, the chemical composition of a real nebular environment would be more complex, allowing many more gaseous and condensed species to form. To test the high-temperature nebular model of fayalite formation, we used the condensation with partial isolation (CWPI) code (Petaev and Wood, 1998, 2000) to carry out equilibrium thermodynamic calculations in a system containing the 18 most abundant elements at a nebular pressure of 10^{-5} bar, dust-to-hydrogen ratios of 10–10 000, and temperatures of 500–1200 K.

The maximum H_2O/H_2 ratio in the gaseous phase of ~3.5 was found in the system enriched in dust by factor of 10 000. This H_2O/H_2 value is within the range of H_2O/H_2 values considered by Hua and Buseck (1995). However, it should be noted that at 1100 K and 10 000× dust enrichment, the system contains ~93 wt% of dust and only ~7 wt% of gas; the gaseous phase consists predominantly of CO_2, CO, H_2O, N_2, and minor amounts of H_2. Obviously, such a system is compositionally very different from a gas-dominated accretionary disk commonly called the solar nebula.

Our calculations show that fayalite, magnetite, and hedenbergite are unstable in the system studied. Instead, ferromagnesian olivine and orthopyroxene with Mg/(Mg + Fe) ratio of <0.5 (depending upon the dust enrichment factor) coexist with magnesiowüstite, Ni-rich metal, and pyrrhotite (at lower temperatures), which is in agreement with calculations of Palme and Fegley (1990). We also find that the molar Fe/SiO ratio in the gaseous phase always exceeds ~200; it becomes progressively higher (up to ~10^7) as the dust-to-hydrogen ratio in the system increases. This means that Fe transport through the gaseous phase would be much more efficient than the SiO transport, resulting in deposition of Fe-rich silicate rims onto the cores of magnesian silicates. We infer that forsterite formed by decomposition of enstatite (reaction (1)) would have exchanged Mg with Fe-rich gas to form ferromagnesian olivine, contrary to the assumption of Hua and Buseck (1995). In fact, reaction (1) would not take place in a nebular environment; instead, enstatite would directly react with Fe vapor to form olivine by reaction

$$Mg_2Si_2O_{6(s)} + 2\,Fe_{(g)} + 2H_2O_{(g)} = 2\,FeMgSiO_{4(g)} + 2\,H_{2(g)} \quad (4)$$

This conclusion is consistent with experimental results of Dohmen *et al.* (1998), who observed the substitution of forsterite by a ferromagnesian olivine because of transport of Fe from metal to olivine *via* a gaseous phase; no ferrous silicates formed on the surface of metal grains.

Thus, the more comprehensive thermodynamic analysis of the high-temperature model of fayalite formation shows that the reactions proposed by Hua and Buseck (1995) could not have taken place in the solar nebula even at unrealistically high dust-to-hydrogen enrichments.

Because the low-temperature gas–solid formation of fayalite in the solar nebula is kinetically prohibited because of very low partial pressures of gaseous SiO (Hua and Buseck, 1995) and Fe, we conclude that formation of fayalite occurred in an asteroidal setting in the presence of aqueous solution (*e.g.*, Krot *et al.*, 1998a,b; Choi *et al.*, 2000).

Manganese and Chromium Age of Fayalite

The evidence for ^{53}Mn in MAC 88107 fayalite is similar to that reported previously for fayalite in the CV3 chondrite Mokoia

(Hutcheon *et al.*, 1998a). If we assume the fayalites in both meteorites formed out of a common initial reservoir (Birck *et al.*, 1999), the shallower slope of the correlation line defined by the data for MAC 88107 corresponds to an age difference of 2 ± 1 Ma between the times of formation of fayalite in the two meteorites. The slope of the MAC 88107 correlation line is very similar to that defined by carbonates in the Orgueil CI chondrite (Endress *et al.*, 1996; Hutcheon and Phinney, 1996), suggesting the contemporaneous formation of fayalite and carbonate, albeit on different parent bodies. Due to the uncertainty in the solar system initial abundance of ^{53}Mn (estimates range from 0.84×10^{-5} (Lugmair and Shukolyukov, 1998) to 4.4×10^{-5} (Birck and Allègre, 1988; Birck *et al.*, 1999)), the age of MAC 88107 fayalite relative to refractory inclusions is difficult to determine accurately. The absolute age of the MAC 88107 fayalite is best determined by comparing the ^{53}Mn/^{55}Mn ratio measured here, $(1.58 \pm 0.26) \times 10^{-6}$, with the angrite value, $(1.25 \pm 0.07) \times 10^{-6}$ (Lugmair and Shukolyukov, 1998). This difference in ^{53}Mn/^{55}Mn corresponds to an age difference of 1.25 ± 0.83 Ma and yields an absolute age of 4559.1 ± 1.0 Ma. The data for MAC 88107 thus extend the evidence for an early onset of aqueous activity on chondrite parent bodies and reinforce the conclusion that liquid water played an important role in the chemical and mineralogical evolution of the first chondritic planetesimals.

Evidence for Growth of Fayalite and Hedenbergite during Low-Temperature aqueous Alteration

Our textural observations indicate that the region of MAC 88107 exposed in the thin section studied largely escaped brecciation and preserved primary accretionary textures, similarly to those previously described in several CM chondrites (Metzler *et al.*, 1992; Hanowski and Brearley, 1997). However, contrary to the CM chondrites, MAC 88107 experienced only minor aqueous alteration (see Transmission Electron Microscopy Study). These unique textural and mineralogical features of MAC 88107 help to distinguish between nebular and asteroidal setting of fayalite and hedenbergite crystallization.

The presence of fayalite-hedenbergite-magnetite veins crosscutting fine-grained rims around chondrules clearly indicates that formation of fayalite and hedenbergite postdated accretion and compaction of the fine-grained rims (Figs. 6 and 7). Some of the veins crosscut fine-grained rims and continue as interconnected layers between neighboring fine-grained rims (Fig. 8). We interpret these observations as a strong evidence for *in situ* growth of fayalite and hedenbergite.

The observations that most of the fayalite-hedenbergite veins crosscut fine-grained chondrule rims and terminate at the boundaries with fine-grained rims around neighboring chondrules could be used as an argument against *in situ* formation of fayalite (M. Weisberg, pers. comm., 2000) and require an explanation.

Fayalite-hedenbergite-magnetite veins commonly start at the oxidized opaque nodules composed of magnetite, Ni-rich sulfides, phosphates, and chromites in the peripheries of the host chondrules. Fayalite and hedenbergite of the veins typically contain small inclusions of magnetite (Figs. 6 and 7). On the basis of these observations, we infer that fayalite and hedenbergite in veins formed by replacement of magnetite. The magnetite veins must have formed during oxidation of metal-sulfide nodules in chondrule peripheries. The oxidation of metal to magnetite results in a large (~2×) volume increase. The volume increase induces high stresses in the adjacent fine-grained rim that eventually breaks to form fractures that would be filled by the growing magnetite. As soon as a fracture crosscuts a fine-grained rim, stress is released and the fracture growth (and magnetite growth) is terminated. However, some of the fractures probably opened into pore space between fine-grained rims and growth of magnetite vein could continue as a layer between the rims. Because MAC 88107 escaped brecciation, which could have produced random fracturing of chondrules and fine-grained rims, the fayalite-hedenbergite-magnetite veins do not crosscut the neighboring fine-grained rims or chondrules. This mechanism explains the observed termination of veins at the boundaries with the neighboring fine-grained rims and the observed continuum between veins and inter-rim fayalite-hedenbergite-bearing layers (Figs. 6i–l and 8).

However, not all fayalite–hedenbergite assemblages in MAC 88107 resulted from the replacement of magnetite. Some of the fayalite and hedenbergite grains appear to fill open spaces in the rock (Fig. 7). These grains must have formed by direct deposition from a fluid percolating through the pore space. Coarse-grained fayalite and hedenbergite between the fine-grained rims (Fig. 8f) and fayalite overgrowing isolated olivine grains (Fig. 9d–g) are generally free of magnetite inclusions and may have a similar origin. The absence of Fe-Mg interdiffusion across the fayalite–fayalitic and forsteritic–olivine boundaries (Fig. 10) is consistent with low-temperature crystallization of this textural type of fayalite.

It has been previously shown that Fe-Mg partitioning (K_D = $(Fe/Mg)^{spinel}/(Fe/Mg)^{olivine}$) between coexisting olivine and Cr-spinel in type-II chondrules is a sensitive indicator of their thermal processing (Johnson and Prinz, 1991). Type-II chondrules in MAC 88107 display K_D values characteristic of equilibration ~1400 °C (Fig. 17), which is consistent with the interpretation that Cr-spinel and olivine co-crystallized from the cooling melt droplets and that the mineral compositions have not been subsequently changed (Johnson and Prinz, 1991). Because fine-grained rims around type-II chondrules in MAC 88107 are crosscut by fayalite-hedenbergite-

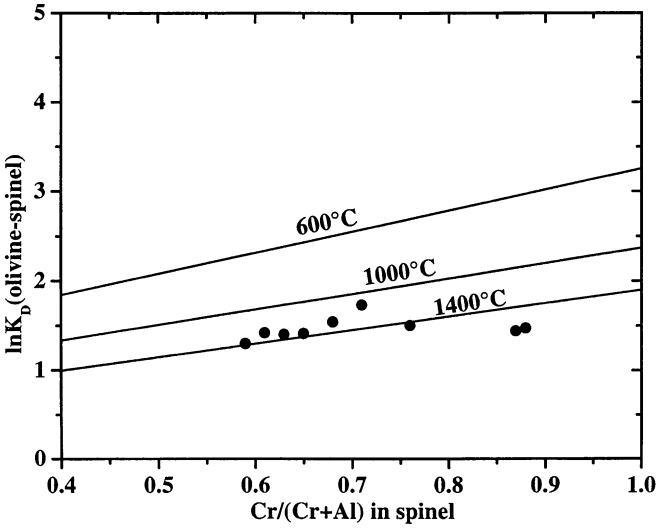

FIG. 17. Iron–magnesian partitioning (K_D = $(Fe/Mg)^{spinel}/(Fe/Mg)^{olivine}$) between coexisting olivine and Cr-spinel in type-II chondrules from MAC 88107. Isotherms are from the AT model of Engi (1983). Most chondrules display K_D values characteristic of equilibration ~1400 °C, which is consistent with the interpretation that Cr-spinel and olivine co-crystallized from the cooling melt droplets and that the mineral compositions have not been subsequently changed.

bearing veins (Fig. 6i,j), we infer that the veins growth did not affect the compositions of olivine and Cr-spinel of the host chondrules. This is consistent with low-temperature origin of fayalite and hedenbergite.

Textural observations and inferred mechanisms of fayalite and hedenbergite formation discussed above (replacement and deposition) suggest that Ca, Si, Fe, and Mn were mobile during alteration and were transported in the fluid phase. The Al-free compositions of hedenbergite indicate extensive fractionation of Ca and Al during the alteration. Such fractionation is commonly observed during low-temperature aqueous alteration of the chondritic meteorites (CI, CM, CR, and CV). Calcium leached out of the primary Ca-rich phases (*e.g.*, anorthitic mesostasis, Ca-Mg-rich pyroxenes) is often deposited as secondary carbonates (*e.g.*, calcite, dolomite), or Ca,Fe-rich silicates (hedenbergite, andradite, or both), whereas Al is typically remains *in situ* to form Ca-free phyllosilicates, such as clays or micas (Keller and Buseck, 1990; Tomeoka and Buseck, 1990; Weisberg *et al.*, 1993; Zolensky *et al.*, 1993). High mobility of Mn required to explain high Mn concentrations in fayalite and hedenbergite can be also achieved during low-temperature aqueous alteration as is suggested by the presence of Mn-rich carbonates in heavily aqueously altered CM and CI chondrites and the Kaidun meteorite (*e.g.*, Endress *et al.*, 1996; Hutcheon *et al.*, 1998a,b). Because mesostasis in many chondrules from MAC 88107 was leached out (Fig. 6) or replaced by Ca-poor phyllosilicates (saponite, serpentine) during aqueous alteration (Browning *et al.*, 1991; Zolensky *et al.*, 1993; this study), it could have been a source of Ca and Si in aqueous solution.

To summarize, our mineralogical, TL, and TEM studies suggest that crystallization of fayalite and hedenbergite in MAC 88107 took place in a planetary setting during relatively low-temperature alteration in the presence of an aqueous solution. Physico–chemical conditions of the alteration are discussed in the following section.

Physico–Chemical Conditions of Aqueous Alteration

Because secondary fayalite, hedenbergite, and magnetite in MAC 88107 are characterized by essentially pure endmember compositions (Fe_2SiO_4, $CaFeSi_2O_6$, and Fe_3O_4), in the discussion below we use the phase diagrams of the Fe–Ca–Si–O–H system calculated previously for the analysis of alteration processes in the least metamorphosed (Bali-like) CV3 chondrites (for details, see Petaev and Mironenko, 1997; Krot *et al.*, 1998a,b).

Figure 18 shows stability fields of magnetite, fayalite, hedenbergite, and andradite at a total pressure of 100 bars and different temperatures, redox conditions (H_2O/H_2 ratio in the gaseous phase equilibrated with an aqueous solution), and compositions of an aqueous solution (Fe^{2+}/Ca^{2+} ratio and SiO_2 concentration). Two conclusions can be drawn from Fig. 18.

First, andradite and magnetite are stable at higher temperatures, at more oxidizing conditions, or both than fayalite and hedenbergite. The lack of andradite in MAC 88107 implies that the aqueous alteration took place at lower temperatures or less oxidizing conditions than those inferred for the CV3 chondrites (Krot *et al.*, 1998a,b). The lower temperature limit of andradite stability depends mainly upon the SiO_2 concentration in an aqueous solution, which itself is a complex function of temperature, pH, and chemical composition of an aqueous solution as well as the mineralogical composition of the rock. A range of SiO_2 concentrations in aqueous solutions can be estimated from the experiments on dissolution of a basaltic glass in different aqueous solutions. Dissolution of a glass in pure water at different temperatures in 90–300 °C range yields secondary alteration assemblage of clays (including saponite) and chlorites and neutral to slightly alkaline aqueous solutions with pH = 6.1 ÷ 9.1 and SiO_2 content of $1.8 \times 10^{-5} \div 1.7 \times 10^{-4}$ mol/l (*e.g.*, Berger *et al.*, 1994; Daux *et al.*, 1997). Dissolution of a glass in Na,Cl-rich solutions compositionally similar to sea water (*e.g.*, Berger *et al.*, 1987) results in similar mineral assemblage of secondary alteration products and higher SiO_2 contents in aqueous solutions ($1.2 \times 10^{-2} \div 3.8 \times 10^{-3}$ mol/l), probably because of acidic nature of these solutions (pH = 2.8 ÷ 4.0). The dissolution experiments also show that the SiO_2 concentration in aqueous solutions is the highest at early stages of alteration and gradually diminishes with time, probably because of precipitation of secondary phases from the aqueous solution.

Two estimates of SiO_2 concentrations in an aqueous solution, approximately 10^{-5} to 10^{-4} mol/l, bracket the temperature limit of andradite stability between ~120 and ~220 °C (Fig. 18c,d). The upper temperature limit (~150 °C) of aqueous alteration of MAC 88107 estimated by Zolensky (1991) from the absence of tochilinite and presence of saponite–serpentine intergrowths in the matrix falls within the temperature range inferred from the thermodynamic analysis.

Second, even at SiO_2 concentration as low as ~10^{-5} mol/l, magnetite is unstable relative to Fe-rich silicates (Fig. 18a). This implies that in the presence of SiO_2 and Ca in an aqueous solution, a replacement of metal by silicates is thermodynamically more favorable. However, our petrographic observations are consistent with the initial oxidation of metal to magnetite, followed by replacement of magnetite by fayalite and hedenbergite. We interpret this alteration sequence as indicative of the lack of transportive medium (an aqueous solution) necessary for redistribution of Fe, Ca, and Si between metal nodules and surrounding silicates rather than of slow dissolution kinetics of silicates at the earliest stages of alteration.

Classification of MacAlpine Hills 88107

On the basis of the bulk O-isotopic composition and x-ray powder diffraction patterns showing olivine and magnetite, but no phyllosilicates, Clayton and Mayeda (1999) suggested that MAC 88107 belongs to the CK group. This classification is inconsistent with its bulk compositional data, which are intermediate between those of CM and CO chondrites (Figs. 2 and 3). Contrary to CK chondrites, MAC 88107 contains phyllosilicates and shows no evidence for even mild thermal metamorphism (Kallemeyn *et al.*, 1991); the TL properties of MAC 88107 also suggest very low petrographic type (about 3.0–3.1). Contrary to CM chondrites, MAC 88107 experienced only minor aqueous alteration, possibly indicating lower water/rock ratio (Clayton and Mayeda, 1999). It appears that this alteration occurred at higher temperatures (approximately 120–220 °C) than that inferred for CM chondrites (~25 °C; Clayton and Mayeda, 1984) and resulted in formation of saponite, serpentine, magnetite, Ni-bearing sulfides, fayalite, and hedenbergite.

On the basis of the bulk compositional data and mineralogical observations described above, we conclude that MAC 88107 is an ungrouped carbonaceous chondrite closely related to the CM-CO clan of meteorites.

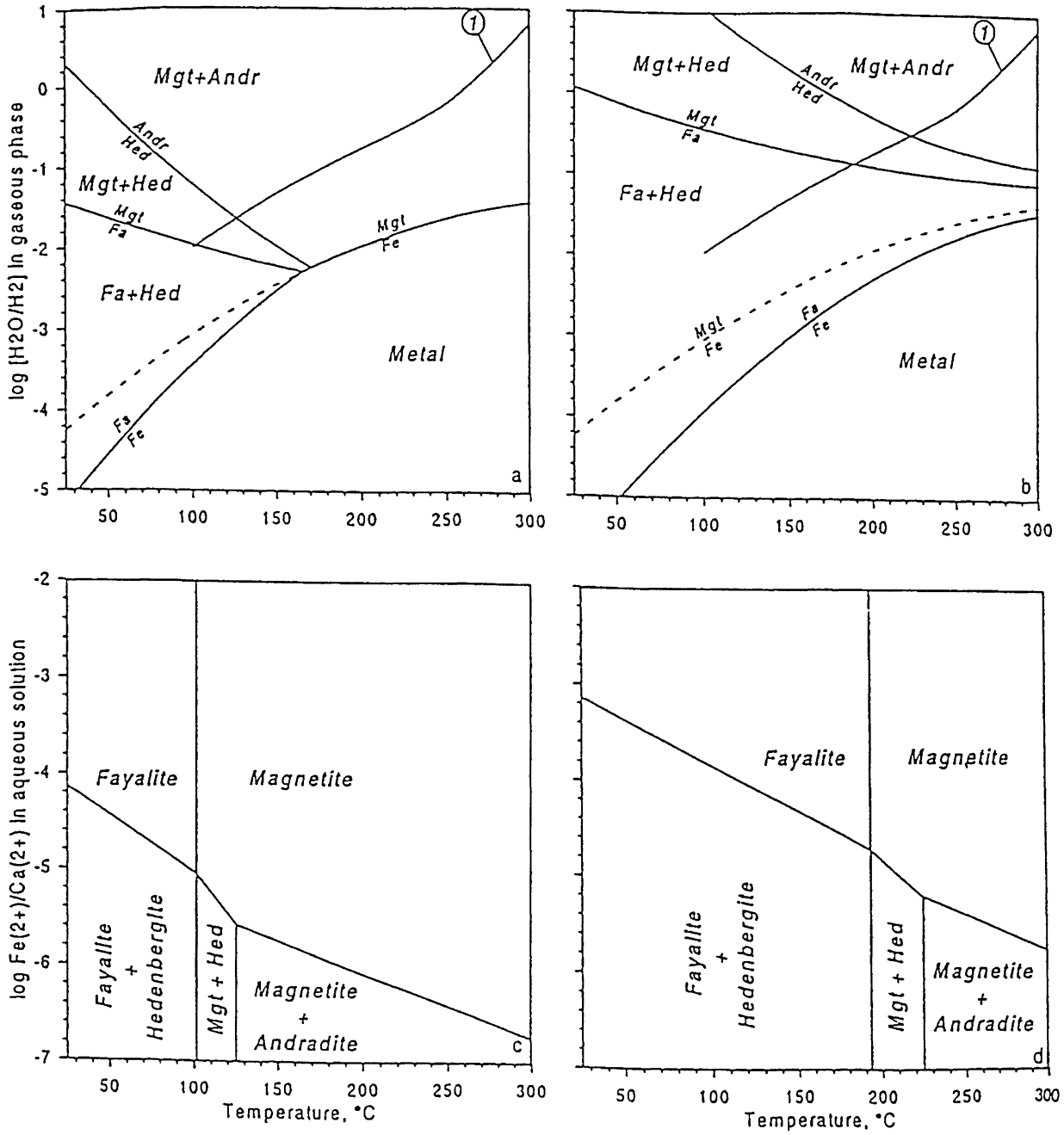

FIG. 18. Equilibrium phase relations in the Fe–Si–Ca–O–H system in the temperature range of 25–300 °C, at a total pressure of 100 bars and activities of SiO_2 in an aqueous solution 10^{-5} (a, c) and 10^{-4} (b, d). Curve labeled "a" represents the H_2O/H_2 ratio in the gaseous phase, which is in equilibrium with liquid water (after Krot *et al.*, 1998a).

Acknowledgements–We thank F. Brenker, T. Fagan, H. Palme, S. Russell, E. Scott, J. Wasson, and M. Weisberg for helpful discussions. This work was supported by NASA grants NAG 5-4212 (K. Keil, P. I.), NAGW 3347 (J. J. Papike, P. I.), and NAGW5-4617 (J. A. Wood, P. T.). This is HIGP publication number 1119 and SOEST publication number 5275. The transmission electron microscope studies were carried out in the Electron Microbeam Analysis Facility, Department of Earth and Planetary Sciences and Institute of Meteoritics, University of New Mexico. Funding was provided by NASA grant NAGW 3347 to J. J. Papike (P. I.).

Editorial handling: J. I. Goldstein

REFERENCES

AKAI J. (1982) High resolution electron microscopic characterization of phyllosilicates and finding of a new type with 11 Å structure in Yamato-74662. *Mem. Natl. Inst. Polar Res., Spec. Issue* **25,** 131–144.

BENOIT P. H., JULL A. J. T., MCKEEVER S. W. S. AND SEARS D. W. G. (1993) The natural thermoluminescence of meteorites: VI. Carbon-14, thermoluminescence and the terrestrial ages of meteorites. *Meteoritics* **28,** 196–203.

BERGER G., SCHOTT J. AND LOUBET M. (1987) Fundamental processes controlling the first stage of alteration of a basalt glass by seawater: An

experimental study between 200 and 320 °C. *Earth Planet. Sci. Lett.* **84,** 431–445.

BERGER G., CLAPAROLS C., GUY C. AND DAUX V. (1994) Dissolution rate of a basalt glass in silica-rich solutions: Implications for long-term alteration. *Geochim. Cosmochim. Acta* **58,** 4875–4886.

BIRCK J-L. AND ALLEGRE C. J. (1988) Mn-Cr isotope systematics and the development of the early solar system. *Nature* **331,** 579–584.

BIRCK J-L., ROTARU M. AND ALLEGRE C. J. (1999) ^{53}Mn-^{53}Cr evolution of the early solar system. *Geochim. Cosmochim. Acta* **63,** 4111–4117.

BREARLEY A. J. (1995) Aqueous alteration and brecciation in Bells, an unusual, saponite-bearing, CM chondrite. *Geochim. Cosmochim. Acta* **59,** 2291–2317.

BREARLEY A. J. (1996) Nature of matrix in unequilibrated chondrites and its possible relationship to chondrules. In *Chondrules and the Protoplanetary Disk* (eds. R. H. Hewins, R. H. Jones and E. R. D. Scott), pp. 137–152. Cambridge Univ. Press, Cambridge, U.K.

BROWNING L. B., ZOLENSKY M. E. AND BARRETT R. (1991) Serpentine and modal compositions of CM chondrites (abstract). *Lunar Planet. Sci.* **22,** 145–146.

CHOI B-G., KROT A. N. AND WASSON J. T. (2000) Oxygen isotopes in magnetite and fayalite in CV chondrites Kaba and Mokoia. *Meteorit. Planet. Sci.* **35,** 1239–1248.

CLAYTON R. N. AND MAYEDA T. K. (1984) The oxygen isotope record in Murchison and other carbonaceous chondrites. *Earth Planet. Sci. Lett.* **67,** 151–166.

CLAYTON R. N. AND MAYEDA T. K. (1999) Oxygen isotope studies of carbonaceous chondrites. *Geochim. Cosmochim. Acta* **63,** 2089–2104.

DAUX V., GUY C., ADVOCAT T., CROVISIER J-L. AND STILLE P. (1997) Kinetic aspects of basaltic glass dissolution at 90 °C: Role of aqueous silicon and aluminum. *Chem. Geol.* **142,** 109–126.

DOHMEN R., CHAKRABORTY S., PALME H. AND RAMMENSEE W. (1998) Solid-solid reactions mediated by a gas phase; an experimental study of reaction progress and the role of surfaces in the system olivine + iron metal. *Am. Mineral.* **83,** 970–984.

ENDRESS M., ZINNER E. AND BISCHOFF A. (1996) Early aqueous activity on primitive meteorite parent bodies. *Nature* **379,** 701–703.

ENGI M. (1983) Equilibria involving Al-Cr spinel: Mg-Fe exchange with olivine. Experiments, thermodynamic analysis, and consequences for geothermometry. *Am. J. Sci.* **283-A,** 29–71.

HANOWSKI N. P. AND BREARLEY A. J. (1997) Transmission electron microscope observations of advanced silicate alteration in chondrules of the CM carbonaceous chondrite, Lewis Cliff 90500 (abstract). *Meteorit. Planet. Sci.* **32 (Suppl.),** A56.

HANOWSKI N. P. AND BREARLEY A. J. (2000) Aqueous alteration of chondrules in the CM carbonaceous chondrite, Allan Hills 81002: Implications for parent body alteration. *Geochim. Cosmochim. Acta* (in press).

HARTMANN L. (1996) Astronomical observations of phenomena in protostellar disks. In *Chondrules and the Protoplanetay Disk* (eds. R. H. Hewins, R. H. and E. R. D. Scott), pp. 13–21. Cambridge Univ. Press, Cambrdidge, U.K.

HASHIMOTO A. (1992) The effect of H_2O gas on volatilities of planet-forming major elements; I. Experimental determination of thermodynamic properties of Ca-, Al-, and Si-hydroxide gas molecules and its application to the solar nebula. *Geochim. Cosmochim. Acta* **56,** 511–532.

HUA X. AND BUSECK P. R. (1995) Fayalite in the Kaba and Mokoia carbonaceous chondrites. *Geochim. Cosmochim. Acta* **59,** 563–578.

HUA X., WANG J. AND BUSECK P. R. (2000a) ^{53}Mn-^{53}Cr dating of fayalite formation in the Kaba and Mokoia CV3 carbonaceous chondrites (abstract). *Lunar Planet. Sci.* **31,** #1091, Lunar and Planetary Institute, Houston, Texas, USA (CD-ROM).

HUA X., WANG J. AND BUSECK P. R. (2000b) Silicon-isotopic abundances in silicate minerals from the Kaba and Mokoia CV3 carbonaceous chondrites (abstract). *Meteorit. Planet. Sci.* **35 (Suppl.),** A78.

HUTCHEON I. D. AND PHINNEY D. L. (1996) Radiogenic ^{53}Cr* in Orgueil carbonates; chronology of aqueous activity on the CI parent body (abstract). *Lunar Planet. Sci.* **27,** 577–578.

HUTCHEON I. D., KROT A. N., KEIL K., PHINNEY D. L. AND SCOTT E. R. D. (1998a) ^{53}Mn-^{53}Cr dating of fayalite formation in the CV3 chondrite Mokoia: Evidence for asteroidal alteration. *Science* **282,** 1865–1867.

HUTCHEON I. D., WEISBERG M. K., PHINNEY D. L., ZOLENSKY M. E., PRINZ M. AND IVANOV A. V. (1998b) Radiogenic ^{53}Cr Kaidun carbonates: Evidence for very early aqueous activity (abstract). *Lunar Planet. Sci.* **30,** #1722, Lunar and Planetary Institute, Houston, Texas, USA (CD-ROM).

JOHNSON C. A. AND PRINZ M. (1991) Chromite and olivine in type II chondrules from carbonaceous and ordinary chondrites: Implications for thermal histories and group differences. *Geochim. Cosmochim. Acta* **55,** 893–925.

KALLEMEYN G. W. (1992a) A carbonaceous chondrite grouplet from MacAlpine Hills, Antarctica (abstract). *Proc. NIPR Symp. Antarct. Meteorites* **6,** 91–92.

KALLEMEYN G. W. (1992b) A carbonaceous chondrite grouplet with affinities to the CM-CO clan (abstract). *Meteoritics* **27,** 240–241.

KALLEMEYN G. W. AND WASSON J. T. (1982) The compositional classification of chondrites: III. Ungrouped carbonaceous chondrites. *Geochim. Cosmochim. Acta* **46,** 2217–2228.

KALLEMEYN G. W. AND WASSON J. T. (1985) The compositional classification of chondrites: IV. Ungrouped chondritic meteorites and clasts. *Geochim. Cosmochim. Acta* **49,** 261–270.

KALLEMEYN G. W., RUBIN A. E., WANG D. AND WASSON J. T. (1989) Ordinary chondrites: Bulk compositions, classification, lithophile-element fractionations, and composition-petrographic type relationships. *Geochim. Cosmochim. Acta* **53,** 2747–2767.

KALLEMEYN G. W., RUBIN A. E. AND WASSON J. T. (1991) The compositional classification of chondrites: V. The Karoonda (CK) group of carbonaceous chondrites. *Geochim. Cosmochim. Acta* **55,** 881–892.

KALLEMEYN G. W., RUBIN A. E. AND WASSON J. T. (1994) The compositional classification of chondrites: VI. The CR carbonaceous chondrite group. *Geochim. Cosmochim. Acta* **58,** 2873–2888.

KALLEMEYN G. W., RUBIN A. E. AND WASSON J. T. (1996) The compositional classification of chondrites: VII. The R chondrite group. *Geochim. Cosmochim. Acta* **60,** 2243–2256.

KELLER L. P. AND BUSECK P. R. (1990) Aqueous alteration in the Kaba CV3 carbonaceous chondrite. *Geochim. Cosmochim. Acta* **54,** 2113–2120.

KROT A. N. AND TODD C. S. (1998) Metal-carbide-magnetite-fayalite association in a Bali-like clast in the reduced CV3 chondrite breccia Vigarano (abstract). *Meteorit. Planet. Sci.* **34 (Suppl.),** A88–A89.

KROT A. N., PETAEV M. I., SCOTT E. R. D., CHOI B-G., ZOLENSKY M. E. AND KEIL K. (1998a) Progressive alteration in CV3 chondrites: More evidence for asteroidal alteration. *Meteorit. Planet. Sci.* **33,** 1065–1085.

KROT A. N., ZOLENSKY M. E., KEIL K., SCOTT E. R. D. AND NAKAMURA K. (1998b) Secondary Ca-Fe-rich minerals in the Bali-like and Allende-like oxidized CV3 chondrites and Allende dark inclusions. *Meteorit. Planet. Sci.* **33,** 623–645.

LARIMER J. W. AND WASSON J. T. (1988) Refractory lithophile elements. In *Meteorites and the Early Solar System* (eds. J. F. Kerridge and M. S. Matthews), pp. 395–415. Univ. Arizona Press, Tucson, Arizona, USA.

LUGMAIR G. W. AND SHUKOLYUKOV A. Y. (1998) Early solar system timescales according to ^{53}Mn-^{53}Cr systematics. *Geochim. Cosmochim. Acta* **62,** 2863–2886.

MASON B. (1988) Petrographic descriptions. *Antarctic Meteorite Newsletter* **11,** 34.

MASON B. (1989) Petrographic descriptions. *Antarctic Meteorite Newsletter* **12,** 20.

METZLER K., BISCHOFF A. AND STÖFFLER D. (1992) Accretionary dust mantles in CM chondrites: Evidence for solar nebula processes. *Geochim. Cosmochim. Acta* **56,** 2873–2897.

PALME H. AND FEGLEY B., JR. (1990) High-temperature condensation of iron-rich olivine in the solar nebula. *Earth Planet. Sci. Lett.* **101,** 180–195.

PETAEV M. I. AND BREARLEY A. J. (1994) Exsolution of ferromagnesian olivine in the Divnoe meteorite. *Science* **226,** 1545–1547.

PETAEV M. I. AND MIRONENKO M. V. (1997) Thermodynamic modeling of aqueous alteration in CV chondrites (abstract). In *Workshop on Parent-Body and Nebular Modification of Chondritic Materials* (eds. M. E. Zolensky, A. N. Krot and E. R. D. Scott), pp. 49–50. LPI Tech. Rep. No. **97-02,** Part 1, Lunar and Planetary Institute, Houston, Texas, USA.

PETAEV M. I. AND WOOD J. A. (1998) The condensation with partial isolation (CWPI) model of condensation in the solar nebula. *Meteorit. Planet. Sci.* **33,** 1123–1137.

PETAEV M. I. AND WOOD J. A. (2000) The condensation origin of zoned metal grains in Bencubbin/CH-like chondrites: Thermodynamic model (abstract). *Lunar Planet. Sci.* **31,** #1608, Lunar and Planetary Institute, Houston, Texas, USA (CD-ROM).

SCOTT E. R. D., RUBIN A. E., TAYLOR G. J. AND KEIL K. (1988) Primitive material surviving in chondrites: Matrix. In *Meteorites and the Early Solar System* (eds. J. F. Kerridge and M. S. Matthews), pp. 718–745. Univ. Arizona Press, Tucson, Arizona, USA.

SCOTT E. R. D., LOVE S. G. AND KROT A. N. (1996) Formation of chondrules and chondrites in the protoplanatery nebula. In *Chondrules and the Protoplanetay Disk* (eds. R. H. Hewins, R. H. Jones and E. R. D. Scott), pp. 87–99. Cambridge Univ. Press, Cambridge, U.K.

SEARS D. W. G., SEARS H. AND MAYERS B. M. (1990) The natural TL survey of the 1987/1988 Antarctic meteorite collections; pairing, an

unusual carbonaceous chondrite group and the lunar meteorites (abstract). *Lunar Planet. Sci.* **21,** 1121–1122.

SEARS D. W. G., HASAN F. A., BATCHELOR J. D. AND LU J. (1991) Chemical and physical studies of type 3 chondrites: XI. Metamorphism, pairing, and brecciation of ordinary chondrites. *Proc. Lunar Planet. Sci. Conf.* **21st,** 493–512.

TOMEOKA K. AND BUSECK P. R. (1990) Phyllosilicates in the Mokoia CV carbonaceous chondrite: Evidence for aqueous alteration in an oxidizing condition. *Geochim. Cosmochim. Acta* **54,** 1745–1754.

WASSON J. T. AND KROT A. N. (1994) Fayalite-silica association in unequilibrated ordinary chondrites—Evidence for aqueous alteration on a parent body. *Earth Planet. Sci. Lett.* **122,** 403–416.

WEISBERG M. K., PRINZ M., CLAYTON R. N. AND MAYEDA T. K. (1993) The CR (Renazzo-type) carbonaceous chondrite group and its implications. *Geochim. Cosmochim. Acta* **57,** 1567–1586.

WEISBERG M. K., PRINZ M., CLAYTON R. N. AND MAYEDA T. K. (1997) CV3 chondrites; three subgroups, not two (abstract). *Meteorit. Planet. Sci.* **32 (Suppl.),** A138–A139.

ZOLENSKY M. E. (1991) Mineralogy and matrix composition of "CR" chondrites Renazzo and EET 87770 and ungrouped chondrites Essebi and MAC 87300 (abstract). *Meteoritics* **26,** 414.

ZOLENSKY M. E., BARRETT R. AND BROWNING L. B. (1993) Mineralogy and composition of matrix and chondrule rims in carbonaceous chondrites. *Geochim. Cosmochim. Acta* **57,** 3123–3148.